

Scuola di Scienze
Dipartimento di Fisica e Astronomia
Corso di Laurea Magistrale in Fisica

Dosimetric characterization of GafChromic EBT3 films in Volumetric Modulated Arc Therapy (VMAT) radiotherapy treatments

Relatore:

Prof.ssa Paola Fantazzini

Presentata da:

Eleonora Rossi

Correlatori:

Dott.ssa Marcella Palombarini

Dott.ssa Silvia Ricci

Abstract

Questo lavoro di tesi, svolto presso l'Unità Operativa di Radioterapia dell'Ospedale Bel-laria di Bologna, si pone l'obiettivo di caratterizzare dal punto di vista dosimetrico i film radiocromici GafChromic EBT3 al fine di implementarne l'utilizzo clinico nell'ambito dei controlli di qualità su piani di trattamento radioterapici VMAT (Volumetric Modulated Arc Therapy).

I controlli di qualità per trattamenti VMAT sono attualmente effettuati grazie ad un sistema fantoccio-detector a camere a ionizzazione, Octavius 4D, in grado di ricostruire in maniera molto accurata la distribuzione di dose tridimensionale depositata su tutto il volume del fantoccio stesso. Nonostante ciò, la risoluzione spaziale offerta da questo strumento risulta limitata in particolari casi in cui è necessario conoscere la distribuzione di dose rilasciata ai tessuti con precisione inferiore a qualche millimetro, mentre il vero punto di forza della dosimetria a film risiede proprio nella elevata risoluzione spaziale.

Con il seguente lavoro abbiamo voluto testare le pellicole EBT3 nella pratica della dosimetria clinica su piani altamente modulati quali i VMAT, osservando la risposta del film rispetto a quella del sistema dosimetrico attualmente impiegato e procedendo per crescenti livelli di difficoltà dei piani irradiati, in modo tale da consolidare la procedura sperimentale.

Abbiamo osservato che, in termini di indice gamma, il più usato per la comparazione quantitativa di mappe di dose, il passing rate nel confronto tra piani di trattamento calcolati e misurati con il sistema Octavius è del 100% per proiezioni bidimensionali e del 99.7% su ricostruzioni tridimensionali (entro limiti descritti dettagliatamente nel paragrafo 3.1). Al contrario, le pellicole raggiungono in un unico caso un passing rate superiore al 95%, soglia di accettabilità nella pratica clinica. Tuttavia, è stato possibile mostrare l'efficacia delle pellicole nella ricostruzione di profili di dose accurati, evidenziando la loro superiorità rispetto alla tecnica dosimetrica correntemente utilizzata per quanto concerne la risoluzione spaziale di dose.

Contents

1	Volumetric Modulated Arc Therapy (VMAT) in radiation therapy treatments	6
1.1	Introduction to radiotherapy	6
1.1.1	Interaction of photons with matter	8
1.1.2	Definition of tumor and target volumes	11
1.1.3	The treatment planning system	13
1.2	Properties of the linear accelerator	14
1.2.1	The accelerating structure	15
1.2.2	The treatment head	17
1.3	VMAT treatments	20
1.4	Quality assurance: pre-treatment tests	21
2	Materials	22
2.1	Farmer ionization chamber	22
2.2	The Octavius system	25
2.2.1	Octavius detector 729	25
2.2.2	Octavius 4D	26
2.2.3	VeriSoft	28
2.3	Film dosimetry with GafChromic EBT3	29
2.3.1	EBT3 films	29
2.3.2	Scanner	30
2.3.3	FilmQA Pro	33
3	Methods for dose verification	34
3.1	The gamma evaluation method	34
3.2	Dose verification with the Octavius system	36
3.2.1	Two dimensional array	36
3.2.2	Octavius 4D phantom	38
3.3	Dose verification with EBT3 films	40
3.3.1	Dose calibration	40
3.3.2	2D plan	42

3.3.3	4D plan	43
4	Results and discussion	45
4.1	Comparison of 2D dose maps	45
4.1.1	Uniform flat field	45
4.1.2	Modulated plans	49
4.2	Comparison of 4D dose maps	53
4.2.1	Irradiation without Octavius system rotation	53
4.2.2	Irradiation with Octavius system rotation	55
4.3	Discussion	57
A	Scanning protocol	60

Introduction

Radiation therapy is one of the most common treatments for cancer. It uses high-energy particles or waves to destroy or damage cancer cells. The main concern of radiotherapy is to deposit as much dose as possible to cancer cells while preserving the healthy tissue surrounding the tumoral mass. Recently, advancements in this field improved the techniques for beam delivering, making it possible to project highly modulated treatment plans, such as VMAT, capable of targeting the tumoral cells very well.

The employ of VMAT treatments in clinical practice carries with it the need of reliable quality assurance, to make sure that the delivery of such complex calculated dose distributions are correctly deposited to the tissue, within clinically acceptable limits. This task is accomplished employing phantoms made of tissue-equivalent material and detectors to simulate the delivery of treatment plans before delivering them to patients.

The purpose of this work, carried out at the *Radiotherapy division of Ospedale Bel-laria (Bologna)*, is to compare two different dosimetry systems: the integrated phantom-detector Octavius 4D, currently employed, and film dosimetry with GafChromic EBT3 for quality assurance of VMAT treatments.

Chapter 1 is an overview on the basics of radiation therapy. In particular, we introduce the topic by describing how radiation therapy is typically delivered in a hospital and the workflow generally followed in clinical practice. Then, we examine the physical interactions at the bottom of this technique and explain in detail the structure and functioning of the linear accelerator (linac) employed to produce photons. We also have a glance at VMAT treatments in particular and the importance of quality assurance tests.

The following chapter provides a detailed description of the experimental equipment we employed to perform our measures: from the ionization chambers array detector for bidimensional dose reconstruction to the Octavius 4D system and all the tools needed for the implementation of film dosimetry, including a mention to VeriSoft and FilmQA Pro, the software for dose distribution analysis.

Chapter 3 introduces a method to quantitatively compare dose distributions (the gamma evaluation method) and follows with the description of the experimental setups we employed to perform our measures for the reconstruction of bidimensional and tridimensional dose distributions.

To conclude, the last chapter contains a critical discussion on the data we obtained, that are in turn presented and evaluated in terms of gamma value.

Chapter 1

Volumetric Modulated Arc Therapy (VMAT) in radiation therapy treatments

1.1 Introduction to radiotherapy

Radiation therapy is a common technique with respect to cancer treatment. In clinical practice, it could be associated with chemotherapy cycles and surgery. It consists in delivering high energy ionizing radiation to the patient, aiming to kill neoplastic cells or at least prevent their proliferation and, in the meantime, preserving normal tissue from radiation damage.

If the absorbing medium consists of body tissue, in fact, sufficient energy may be deposited within the cells, damaging their DNA and thus altering their biological functions. Depending on the damage importance, the cell can completely recover, transmit a mutation or eventually die. Generally, if only one strand of the DNA chain is damaged, the other strand serves as a template for repair, as the nucleotides of the two are complementary. Otherwise, if a double-strand break takes place either the cell dies or, most rarely, mutates transmitting the mutation to daughter cells.

Cancer cells have been proved to have a different proliferation rate to the one observed for healthy cells. As a result, the latter are less sensitive to radiation damage, making the treatment more selective for target tissue. The graph in Figure 1.1 illustrates the dose vs effect curves for tumoral tissue and normal tissue defined as the Tumor Control Probability (TCP) and Normal Tissue Complication Probability (NTCP) respectively. While both curves are sigmoidal, the NTCP one is usually steeper than the TCP curve, as normal cells are more sensitive to radiation damage.

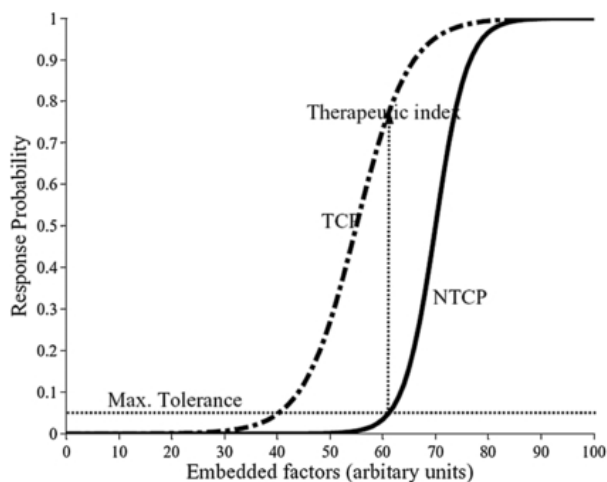


Figure 1.1: Sigmoidally shaped response curves (for TCP and NTCP) are constructed as a function of a linear weighting of various factors, for a given dose distribution, which may include multiple dose-volume metrics as well as clinical factors. The units of the x-axis may be thought of as “equivalent dose” units [8].

Radiotherapy is thus employed when the probability to cause radiation damage to tumoral tissue is by far higher than the probability to damage normal tissue.

Radiation therapy treatments can be involved in a number of situations: when the tumoral cells have to be completely destroyed thus aiming to recovery (sometimes in association with chemotherapy cycles); after surgery, to prevent potentially residual cells from proliferating; to mitigate symptoms if the patient is terminal and cannot recover.

Several types of radiotherapy exist (external beam radiotherapy, brachytherapy, metabolic radiation therapy, intra-operative radiation therapy) but we will focus here on external beam radiation therapy: the body is irradiated from outside thanks to a linear accelerator.

It is important to compromise between side effects and efficacy when it comes to planning treatments. A number of expedients have been implemented through years in order to maximize the efficiency of treatments: limit the total irradiated dose, even if tumoral tissue is underexposed to avoid side effects; fractionate the total dose to be irradiated in separate daily sessions (normal cells can recover from one session to another, reducing the damage to healthy tissue surrounding the target); irradiate the target from different directions.

When a patient starts a treatment, a preliminar CT (Computed Tomography) scan

is taken, in order to precisely localize the target. The patient has to keep the exact same position over different sessions, so, in order to avoid errors, when the target is delineated, small reference points are permanently drawn on the skin and different immobilizing tools are employed. Moreover, prior to every session, a CT scan is taken in order to compare it to the preliminar one and detect eventual movements of the target. Generally, daily sessions for five days in a row is the standard fractioning, but exceptions are possible: sometimes higher dose irradiations are planned keeping the sessions separated by two or more days, sometimes lower dose irradiations are erogated in the same day with a six hours (minimum) break between them.

1.1.1 Interaction of photons with matter

With regard to the type of radiation employed in radiotherapy treatments, photons and electrons are the first choice. As a result of interaction between photons and matter, energy is transferred to the medium through which the beam passes. At first, the energy transfer involves the ejection of electrons from the atoms of the absorbing medium. These electrons transfer their energy by producing ionization and excitation of the atoms along their paths. This is the reason why electrons are called directly ionizing radiations, while photons are referred to as indirectly ionizing radiation. We will focus here on the interactions of photons with matter.

The attenuation of a monoenergetic beam of photons passing through an absorber is proportional to the number of incident photons (N) and the thickness of the absorber (dx):

$$dN \propto Ndx \quad (1.1)$$

The constant of proportionality is called the *linear attenuation coefficient*, μ . This yields to the following equation for beam attenuation:

$$I(x) = I_0 e^{-\mu x} \quad (1.2)$$

where $I(x)$ is the beam intensity in function of depth.

Four different processes give a contribution to attenuation: *coherent scattering*, *photoelectric effect*, *Compton effect* and *pair production*. Thus the attenuation coefficient is given by the sum of four coefficients:

$$\frac{\mu}{\rho} = \frac{\sigma_{coh}}{\rho} + \frac{\tau}{\rho} + \frac{\sigma_c}{\rho} + \frac{\pi}{\rho} \quad (1.3)$$

where σ_{coh} , τ , σ_c and π are the attenuation coefficients for coherent scattering, photoelectric effect, Compton effect, pair production respectively, while ρ is the density of the absorber.

- **Coherent scattering (or Rayleigh scattering)**

When the incident photon comes across an electron, it sets it into oscillation. Then, the electron irradiates the energy it has absorbed in the form of another photon with the same frequency as the first one. As displayed in Figure ??, no energy is absorbed by the atom due to this process. Scattering is the only effect.

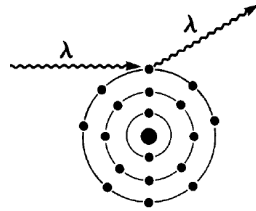


Figure 1.2: Coherent scattering

The probability for coherent scattering to take place is high only for high atomic number materials and low energy photons. As a consequence, this is not a process of interest for the purpose of radiotherapy.

- **Photoelectric effect**

The photoelectric effect occurs when the interaction between the incident photon and the atom of the absorber leads to the ejection of an orbital electron from the atom. The energy of the electron equals to the difference between the energy of the photon $h\nu$ (that is completely released to the atom) and the binding energy of the electron E_B . A vacancy is formed, bringing the atom to an excited state, consequently another electron from an outer shell fills the vacancy, thus the atom can return back to its ground state emitting a characteristic x-ray. Also, the emission of Auger electrons is possible within the process. These are monoenergetic electrons emitted as characteristic x-rays are absorbed internally by the atom.

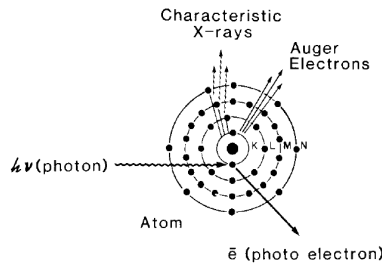


Figure 1.3: Photoelectric effect

As for biologic absorbers, the energy of characteristic x-rays is sufficiently low to assume that all the energy is deposited within the atom.

- **Compton effect**

In this case the incident photon interacts with an orbital electron that is approximately free, in the sense that the energy of the photon is much higher than the binding energy of the electron. As a result, both electron and photon are scattered. This phenomenon is different from coherent scattering because of the energy transfer between the photon and the electron.

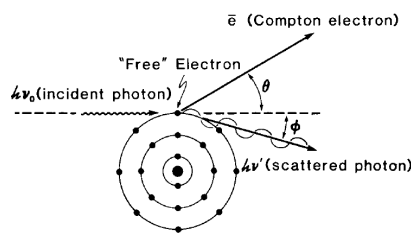


Figure 1.4: Compton effect

- **Pair production**

When the energy of the photon is at least 1.02 MeV, pair production can occur. In this case, the photon releases all its energy due to the interaction with the electromagnetic field of the atomic nucleus and creates an electron and a positron.

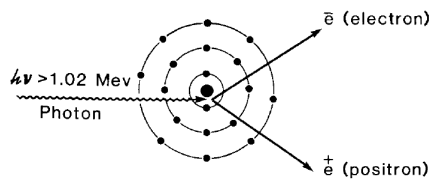


Figure 1.5: Pair production

The threshold energy is set at 1.02 MeV because the rest mass energy of the electron is 0.511 MeV

The cross section for each of the phenomena described above is not constant, in fact a dependence exists between the probability for each process to occur and the energy and atomic number of the photon and the absorber respectively.

The graph in Figure 1.6 illustrates this dependence:

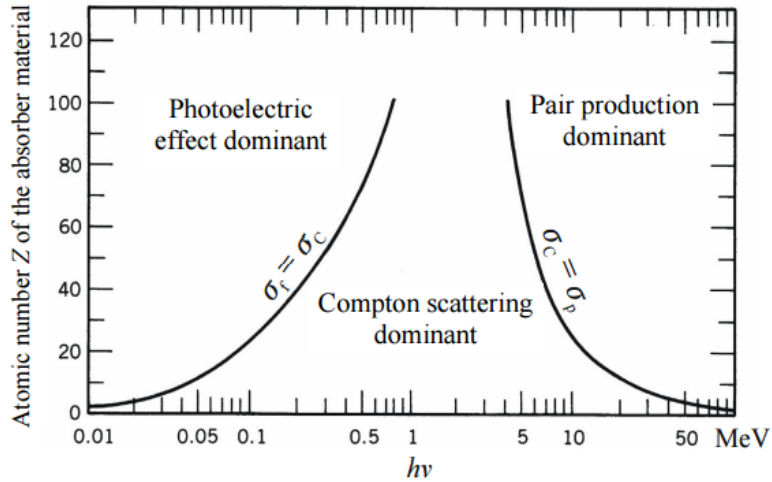


Figure 1.6: Cross section for photoelectric effect, Compton effect and pair production in function of energy and atomic number

The energy range in radiotherapy treatments is between 1 MeV and 20 MeV and the atomic numbers of soft tissue and bones spread approximately from 6 to 12, thus the most common processes are Compton effect and pair production.

1.1.2 Definition of tumor and target volumes

When delivering a treatment, several rules should be followed in determining the volume to be irradiated. The International Commission on Radiation Units and Measurements (ICRU) provides universally accepted guidelines for prescribing, recording and reporting dose for radiation treatments [12].

For this purpose, it is necessary to introduce the definitions of several volumes related to both tumor and normal tissue. Delineation of these volumes is compulsory when planning the treatment, as dose prescription cannot be carried out without specification of target volumes and volumes of normal tissue at risk.

The *Gross Tumor Volume* (GTV) is defined as the macroscopic tumoral volume. It can be delineated on anatomic or functional imaging modalities and both before or during treatment to detect a potential change in the target volume.

The *Clinical Target Volume* (CTV) is defined as the volume containing a demonstrable GTV that must be eliminated. As the CTV is potentially affected by several uncertainties (related to geometrical and/or physiological factors) it is necessary to add a margin

around it. Specifically, an internal margin that takes into account the internal movement of the CTV and a set-up margin related to, for example, a variation in the patient set-up.

The *Planning Target Volume* (PTV) is, by definition, the volume that incorporates the CTV and surrounding margin. Its delineation is performed by means of purely geometrical considerations, in order to ensure that the prescribed dose is effectively delivered to the CTV with acceptable confidence.

Organs at risk (OAR) should be also taken into account, as if irradiated could suffer significant morbidity, with a consequent influence on the treatment planning and/or the dose prescription. Delineation of OARs takes into account possible uncertainties sources (as the CTV) by adding margins that depend on the position and structure of the OAR (i.e. the spinal cord is more critical than the parotid glands thus will require a wider margin).

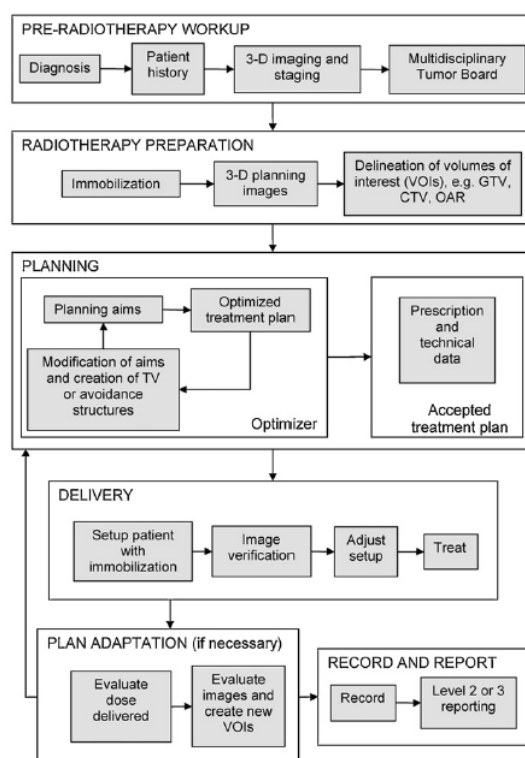


Figure 1.7: Flow chart of a typical course of radiotherapy [12]

Figure 1.7 shows the iterative process known as “optimization”. At first the definition and description of the so-called planning aim is carried out, involving the delineation of the previously introduced volumes and desired absorbed dose values, then a complex beam delivery optimization takes place thanks to the treatment planning system (TPS)

in order to achieve the preset planning aims (or modify them if needed) and eventually a set of finally accepted values to which we refer as “treatment prescription” together with the required technical data represent the accepted treatment plan.

1.1.3 The treatment planning system

The treatment planning system is a software dedicated to dose computation relative to target volumes and OARs. The optimization process is a crucial step when delivering a modulated treatment plan such as VMAT. Dose computation is based on a set of dose values to be delivered for each delineated volume on the reference CT scan. This involves the specification of dose values for target volumes as well as the maximum dose limit for OARs. The software then iteratively modifies the beam intensities to achieve the expected result.

The dose is computed by sampling the delivery at a number of discrete gantry angles. In order to create a satisfactory dose plan with a single arc, it is necessary to optimize the field shapes and beam intensities from a large number of gantry angles. However, the field shapes are restricted in that the MLC leaves must be able to move to their new positions within the time required for the gantry to rotate between samples. On the other hand, the larger the number of sampled gantry angles, the more difficult it is for the TPS to optimize within the MLC leaf motion constraints.

Sometimes, for highly modulated plans, the optimized plan cannot fit the initial dose constraints. When this is the case, the physicist and the doctor decide whether the plan is still acceptable or some constraints have to be modified. When important OARs are involved, such as the spine cord, it is at times necessary to lower the total dose of the treatment to prevent radiation damage from happening.

The TPS software we used for the computation of the calculated treatment plans is Elekta Monaco, installed at the radiotherapy division at Ospedale Bellaria (Bologna). Monaco’s VMAT functionality can optimize single or multiple non-coplanar arcs simultaneously, providing the flexibility and control needed for complex treatment plans such as VMATs. Monaco offers the XVMC Monte Carlo dose engine, for electron and photon, for a continuous arc calculation as a single beam, rather than just dose approximations that occur with many discrete (control point) gantry angle positions.

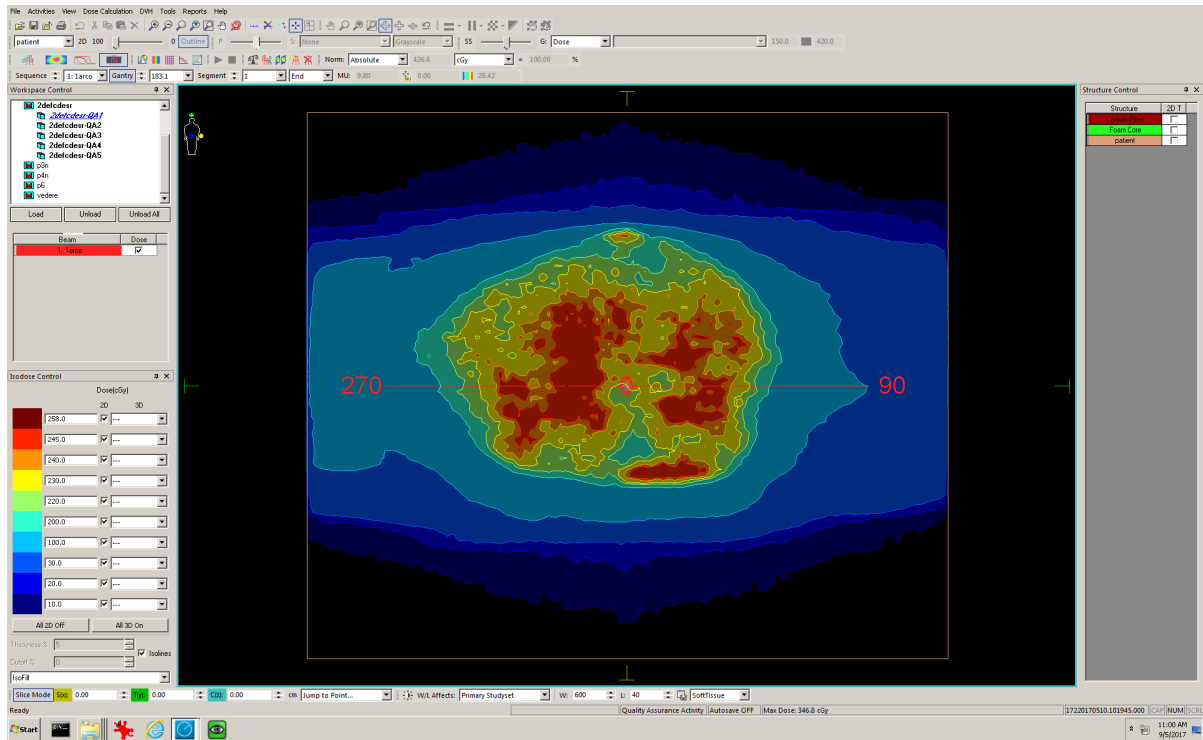


Figure 1.8: Monaco interface. Every color represents a different dose value, as reported in the legend on the left.

When the optimization process has ended, the validated plan is exported to the accelerator’s control software, MosaiQ, and can be delivered.

1.2 Properties of the linear accelerator

The linear accelerator (linac) is a device that uses high-frequency electromagnetic waves to accelerate charged particles such as electrons to high energies through a linear tube. The high-energy electron beam itself can be used for treating superficial tumors, or it can be made to strike a target to produce x-rays for treating deep-seated tumors.

The radiation therapy division at Ospedale Bellaria (Bologna) hosts an Elekta Synergy model equipped with the Agility beam shaping system, where electrons are accelerated by traveling electromagnetic waves of frequency in the microwave region.

The block diagram illustrated in Figure 1.10 shows the main parts of a medical linear accelerator.



Figure 1.9: The linear accelerator installed at Ospedale Bellaria.

1.2.1 The accelerating structure

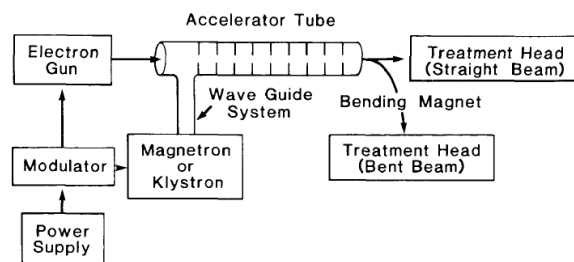


Figure 1.10: Block diagram of a typical linear accelerator [13]

The *power supply* is meant to provide direct current to the *modulator*, which in turn delivers high-voltage pulses to the *magnetron* and the *electron gun*.

The magnetron is a device dedicated to the production of microwave pulses with frequency of about 3000 MHz for each pulse.

Figure 1.11 illustrates the diagram of the cross-section of a typical magnetron.

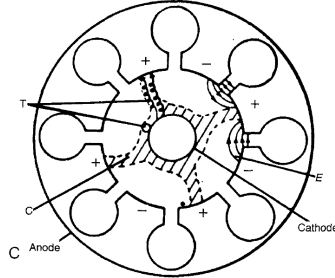


Figure 1.11: Cross-section of a typical magnetron [13]

Its structure is cylindrical, with a central cathode and an external anode with several resonant cavities obtained from a solid piece of copper; the space between the two is evacuated. Electrons are produced by thermoionic emission by means of a filament inserted into the cathode. A static magnetic field and a direct current pulse are then applied perpendicularly to the plane identified by the cross-section of the cavities and between the cathode and the anode respectively. As a result, electrons are accelerated from the cathode towards the anode and move, as a consequence of the magnetic field, in complex spirals towards the cavities, thus emitting radiation in the microwave range. Eventually these microwave pulses are driven to the accelerator structure through the waveguide.

The *waveguide* system injects the pulsed microwaves into the accelerator tube; synchronously, electrons from the electron gun are injected as well.

The *accelerator tube* is a cylindrical structure about 3 m long made up of copper. The tube is internally divided by copper discs or diaphragms with different spacing between them through which the electromagnetic wave passes. Every diaphragm owns a circular cavity to allow the passage of electrons. The electromagnetic wave velocity and the energy it can transfer to electrons depend on the radius of the accelerator tube and on the geometrical properties (radius, thickness, height) of the diaphragms. In the first part of the accelerator tube diaphragms are set closer, aiming to reduce the phase velocity of the electromagnetic wave to that of the electrons. This way, electrons will be located on the wave peak, accelerating along their path by the axial component of the electric field until they reach approximately the speed of light. Accelerating electrons tend to diverge, so a focusing system consisting of focusing coils is needed.

The accelerator tube, as well as the electron gun needs to be set into high vacuum conditions, in order to make sure that the mean free path of electrons is long with respect to the distance electrons travel through the tube. Moreover, a water cooling system is designed to keep the magnetron and accelerator tube temperature constant, thus preventing hazardous termic expansions that would compromise the efficiency of the whole

system .

Accelerated electrons are driven to the treatment head thanks to a system of magnetic fields specifically designed to join up the accelerator tube and the treatment head where the high-Z target is located. When electrons hit the target, X-rays for the actual treatment are produced by bremsstrahlung. The target is thick enough to absorb most of the incident electrons and is water cooled, as hitting electrons would heat it up. The maximum photon energy is equal to that of the incident electrons, but the average photon energy is about one third of it. The Elekta Synergy model provides two mean energy values for the photon beam: 6 MV and 10 MV. Energy is conventionally expressed by megavolts, as if the x-ray beam were produced by a x-ray tube with that voltage between its anode and cathode.

1.2.2 The treatment head

The treatment head is the most important part of a linear accelerator. It is made up of a thick shell of high-density shielding material (i.e. lead, tungsten or alloys) and contains several components.

The diagram in Figure 1.12 illustrates the structure of the Agility treatment head. The electronic beam from the accelerator tube hits the target producing symmetrical x-rays, which pass through a hole in the primary filter group, 12 mm below the target. The primary collimator, made up of a tungsten alloy (density of 18 g/cm^3) then operates as follows: high-energy x-rays pass through Port 1 (containing the differential filter) and Flattening Filter Free (FFF) x-rays pass through Port 2 (which is empty). The secondary filter uniforms the shape of the x-rays beam, which in turn passes through the backscatter plate. The beam profile can be modified thanks to the motorized wedge, then the leaves composing the MLC can give an irregular shape to the beam with respect to the x axis and the y diaphragms can collimate the beam in the y direction with a rectangular shape. Eventually, x-rays cross the mylar layer, which is used to identify the isocenter and position of the wedge thanks to a light field.

The MLC plays a crucial role in the delivering of modulated treatments such as VMATs: it replaces old shielding techniques with a combination of high resolution beam shaping and rapid leaf speeds, allowing higher dose rates to be used for more effective modulation. Moreover, only 0.5% of the dose is transmitted, preventing healthy tissue from receiving an unwanted dose [5]. Figure 1.13 shows a diagram of the Agility MLC.

It is made of two groups of 80 leaves each located perpendicularly to the radiation direction and moving linearly along the beam path. Each group is driven by a dynamic leaf guide that allows for movement at a maximum speed of 3.5 cm/s during the treatment delivery. Leaves are made of a tungsten alloy with density of 18 g/cm^3 and a nominal

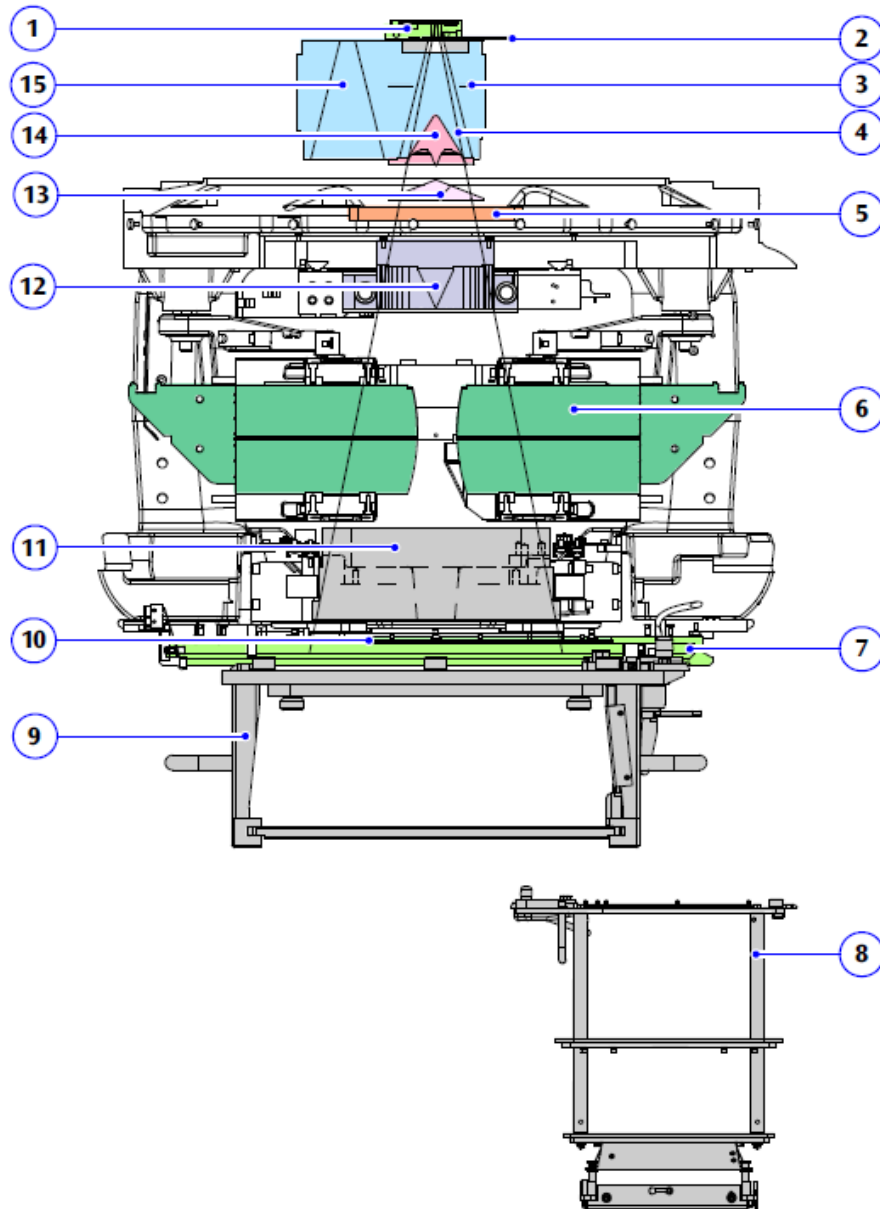


Figure 1.12: Components of the treatment head. (1) Target, (2) primary filter group, (3) primary collimator, (4) port 1, (5) ionizing chamber, (6) MultiLeaf Collimator (MLC), (7) accessories ring, (8) device for electron modality, (9) template holder for adding shielding blocks, optional, (10) Mylar screen, (11) Y diaphragms, (12) motorized wedge including backscatter plate, (13) secondary filter, (14) differential filter, (15) port 2 [11]

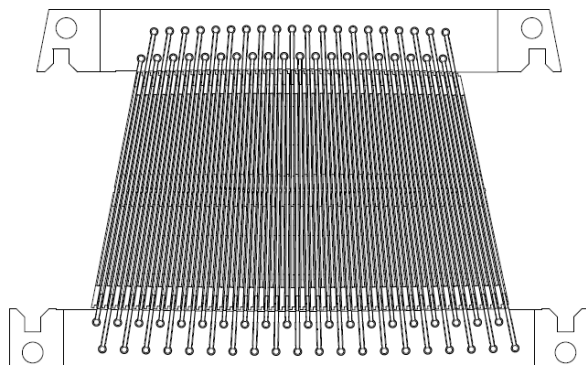


Figure 1.13: Transversal section of the Agility MLC [11]

projected width of 5 mm with reference to the isocenter, thus the largest flat field we can obtain is $40 \times 40 \text{ cm}^2$. A small gap is left between the leaves in order to prevent friction, and their edges are rounded (radius of 170 mm) to optimize the penumbra (80%-20% dose distance). Also, some leaves cannot completely extend to 20 cm, so a more realistic representation of a $40 \times 40 \text{ cm}^2$ flat field is the one displayed in Figure 1.14

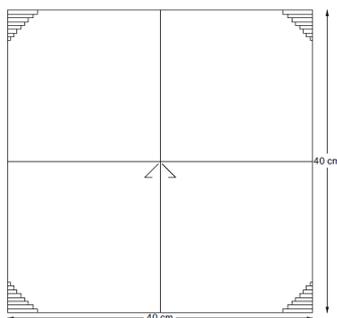


Figure 1.14: Effective limits of the collimator leaves [11]

The components mentioned up until now (magnetron, electron gun, accelerator tube and treatment head) are all assembled on a rotating structure to which we refer to as *gantry*. The movement of the gantry is designed to provide for the radiation source to rotate about a horizontal axis, while the central axis of the treatment head is vertical. The *mechanical isocenter* is thus defined as the meeting point of the two axis described above. This corresponds, within a tolerance of 1 mm for the Agility [11], to the center of the smallest sphere through which radiation beams pass under every condition, known as the *radiation isocenter*. In the following chapters we will always refer to the mechanical isocenter.

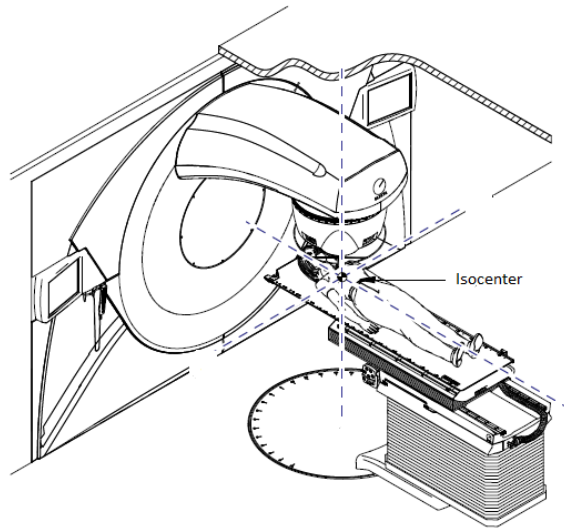


Figure 1.15: Isocenter position [11]

1.3 VMAT treatments

Volumetric-modulated arc therapy (VMAT) is a radiation therapy technique that consists in the delivery of a rotational cone beam with variable shape and intensity. In a VMAT treatment, the gantry moves continuously, with the MLC leaves and dose rate varying throughout the arc. This approach has been proved more effective in terms of time needed for treatment and dose distribution efficiency as well, managing to deliver a lower dose to OARs with respect to older techniques such as IMRT or 3D conformational radiotherapy [24] [4] [22][16].

A lower dose to OARs is a significant improvement and benefit, especially for patients for whom the induction of secondary malignancies may be a factor because of life expectancy. For example, as this is a great concern in pediatric cases, VMAT could be implemented as a great alternative to IMRT or complex cases where proton therapy is not available. Also, shorter overall delivery time has a number of advantages, most importantly in reducing the amount of patient motion that occurs during treatment.

Figure 1.16 shows a comparison between IMRT and VMAT dose distributions. Qualitatively, the VMAT plan is more conformal, with less moderate to high dose in the normal tissue and the total VMAT treatment time was reduced by 8 min with respect to IMRT.

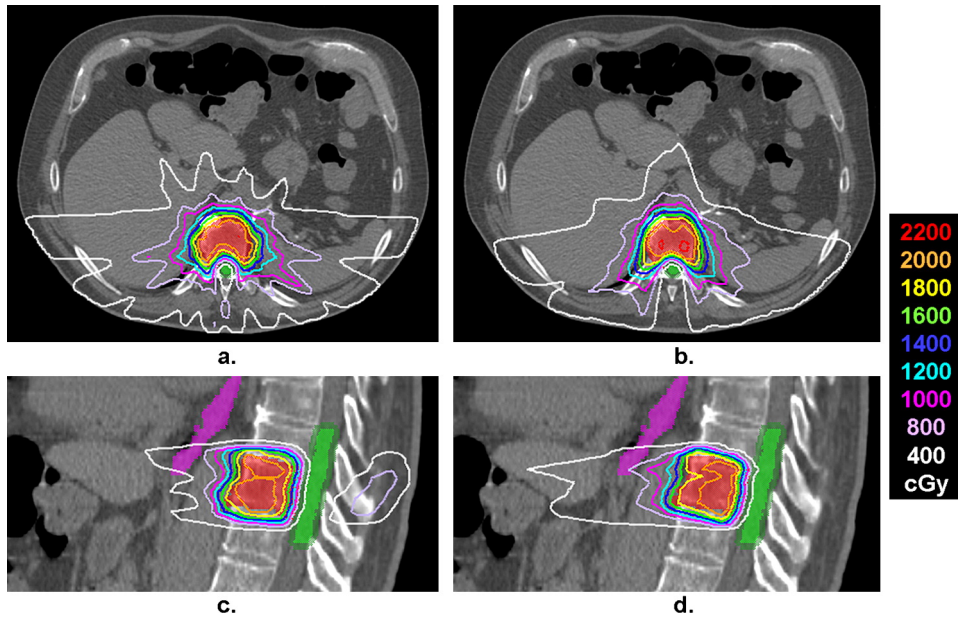


Figure 1.16: Comparison of IMRT (a,c) and VMAT (b,d) dose distributions [16]

1.4 Quality assurance: pre-treatment tests

The term quality assurance (QA) describes a program that is designed to control and maintain the standard of quality set for that program. For radiation oncology, a quality assurance program is essentially a set of policies and procedures to maintain the quality of patient care. The general criteria or standards of quality are usually set collectively by the profession. The primary goal of quality assurance is checking the stability, accuracy and reproducibility of the equipment. Periodical trials should be carried out to make sure that physical parameters describing the above mentioned properties keep their values within acceptable ranges.

IMRT and especially VMAT treatments are far more complex than those of traditional radiotherapy, thus periodical checks on the accelerator and other equipment are no longer sufficient to assure a reliable QA. Medical physicists are then required to carry out pre-treatment measures to make sure that eventual dose discrepancies between the prescribed plan from the TPS and measurements are clinically acceptable.

Chapter 2

Materials

In this chapter we describe all the experimental equipment employed for dosimetric evaluation in different experimental setups. An overview on the software tools for later analysis is also provided.

2.1 Farmer ionization chamber

The first Farmer ionization chamber was designed in 1955 [9], providing a valid secondary standard for x-rays and gamma rays in the whole therapeutic energy range. The chamber was connected to a specific electrometer (to measure ionization charge) and is known as the Baldwin-Farmer substandard dosimeter. Its design was modified in the '70 by Aird and Farmer [2] in order to supply flatter energy response characteristics and less different design from one chamber to another. The diagram in Figure 2.1 represents a section of the one just mentioned.

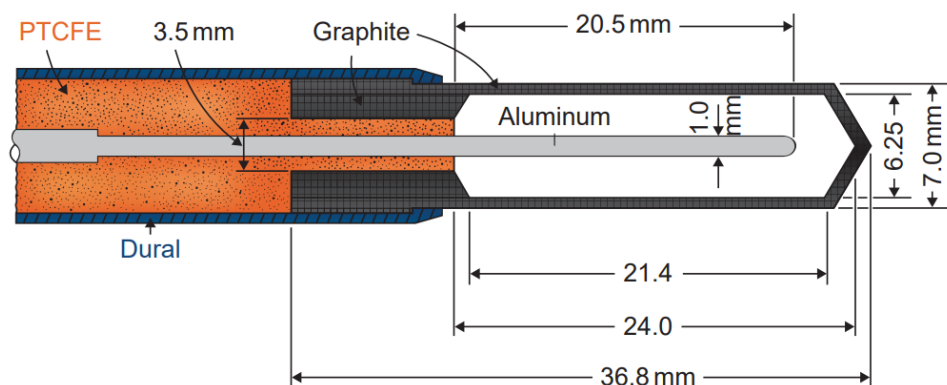


Figure 2.1: Section of a Farmer ionization chamber [2]

The thimble wall is made of pure graphite and the central electrode is of pure aluminum.

The insulator consists of polytrichloroethene. The collecting volume (air cavity volume) of the chamber is nominally 0.6 cm^3 .

Three are the main components of this type of chamber: the central electrode (collector), the thimble wall, and the guard electrode. The collector electrode collects the ionization charge delivering the ionization current to a charge-measuring device, an electrometer. The electrometer is driven by a dual polarity high-voltage source needed to hold the collector at a high bias voltage. When the chamber is exposed, in fact, secondary electrons produced from the interaction of photons with the chamber wall ionize the air in the cavity. Ions thus generated are collected from the collector and the guard. As a result, the charge of the electrodes is reduced, proportionally to the ionization. The thimble is at ground potential and the guard electrode is kept at the same potential as the collector. The guard electrode is a cylindrical conductor needed to prevent the leakage current of any extraneous charge from the collector, as there is no potential difference between the two. The thimble wall is then designed to define the ion-collecting volume, in other words, the mass of air in the cavity that in turn determines the sensitivity of the chamber, expressed as charge measured/unit exposure.

When assessing the performance of a Farmer-type ionization chamber two factors should be taken into account: energy dependence and the stem effect. Energy dependence expresses the change in response with respect to the beam energy and is generally depending on the composition and thickness of the wall material. Stem effect involves the collection of leakage current originating from ionizations that take place in the chamber stem and the cable instead of the air cavity, if they are exposed. The stem effect originating in the stem is directly related to the length of the unguarded stem and the overall amount of stem effect (both from the stem and cable) is a function of energy as well as type of beam (photon or particle). Fully guarded Farmer-type chambers have almost immeasurable stem effect. However, the stem effect must be checked periodically for corrections.

The chamber we used for absolute dose measurements is a PTW waterproof Farmer chamber, model 30013 with a measuring volume of 0.6 cm^3 [21].

This chamber is suitable for measuring doses deposited both from electrons and photons. The nominal photon energy range is from 30 kV to 50 MV, the electron energy range is from 10 MeV to 50 MeV. The wall material is graphite with a protective acrylic cover and the electrode is made of aluminum. Figure 2.3 displays the diagram of the chamber described above.



Figure 2.2: Farmer chamber type 30013 [21]

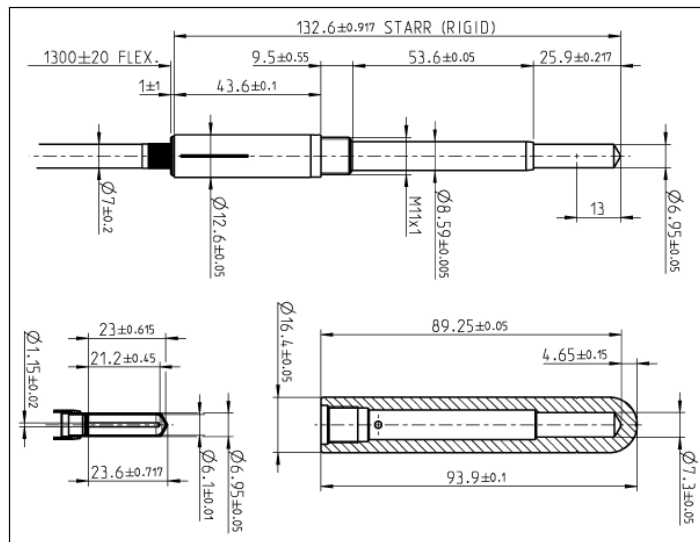


Figure 2.3: Drawing of the Farmer chamber type 30013 (all dimensions are in mm) [21]

2.2 The Octavius system

The PTW Octavius 4D system consists of a cylindrical polystyrene phantom (density 1.05 g/cm^3) hosting a detector made of plane-parallel vented ionization chambers (Octavius detector 729) and is suitable for pre-treatment quality assurance on VMAT plans, as it provides a 3D dose reconstruction. Moreover, it is possible to employ the detector alone in order to measure 2D dose distributions. The Octavius system is equipped with the dedicated software VeriSoft for dose distribution analysis.

2.2.1 Octavius detector 729

The Octavius detector 729 (Figure 2.4) provides a matrix of 729 ionizing chambers calibrated with a ^{60}Co source for absolute dose measures.

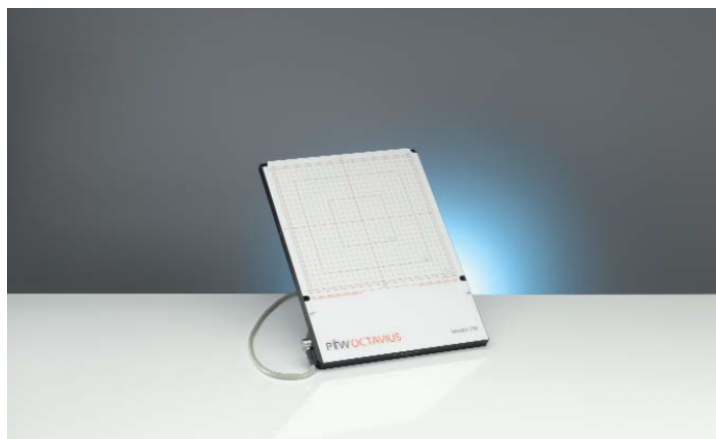


Figure 2.4: Octavius detector 729 [20]

Ionization chambers are suitable for absolute dosimetry as the energy-response curve is flat, as a consequence of their water-equivalent design. In addition, their response is stable with respect to accumulated dose. Effects such as temperature or dose rate dependence can be easily taken into account by means of correction factors (see section 3.2.1).

The vented plane-parallel ion chambers are $5 \text{ mm} \times 5 \text{ mm} \times 5 \text{ mm}$ in size, and the center-to-center spacing is 10 mm . In total there are located 729 chambers in a matrix of 27×27 , providing a maximum field size of $27 \text{ cm} \times 27 \text{ cm}$. Each chamber will give a dose response which is averaged over its volume, as the geometrical dimensions of chambers are finite. The cubic design of PTW's Octavius detector provides minimal angular dependence of the detector's response, as it approaches the ideal spherical geometry (Figure 2.5).

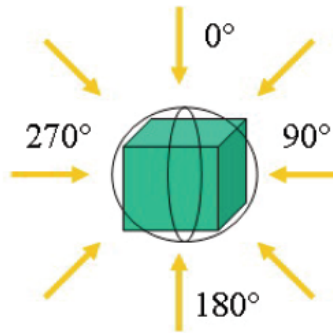


Figure 2.5: Geometrical properties of a cubic ion chamber of PTW’s Octavius detector 729 almost matching a spherical geometry. Arrows indicate the beam direction. [20]

As a result, no correction is needed to take into account effects deriving from the rotation of the gantry. To conclude, an odd number of chambers is chosen so that the geometrical center of the array corresponds to the beam central axis.

2.2.2 Octavius 4D

The Octavius 4D phantom (Figure 2.6) shows a novel approach with respect to QA in modulated treatments such as VMAT.



Figure 2.6: Octavius 4D employed at Ospedale Bellaria (Bologna)

The innovation of this phantom relies on the synchronous rotation of the Octavius with the gantry, measuring the dose inside the entire phantom volume always perpendicularly to the beam direction. The major advantage of this is that angular corrections or detector calibrations to compensate for the directional response of detectors are no longer needed, making the system suitable for clinical routine. Three dimensional angle-dependent dose

distributions are recorded, thus the four-dimensionality.

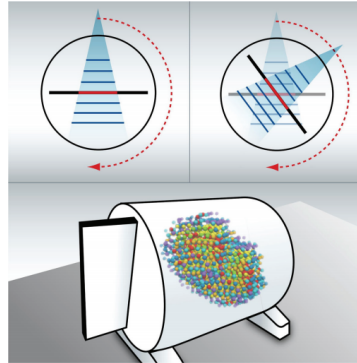


Figure 2.7: Schematic of the rotation of gantry and Octavius [19]

The rotation is provided thanks to a device that connects via bluetooth the gantry inclinometer and the Octavius; once they are matched, only relative angle values are needed, thus reducing error sources. The dose distribution is reconstructed summing up the information from the rotation unit and the detector interface (see Figure 2.8).

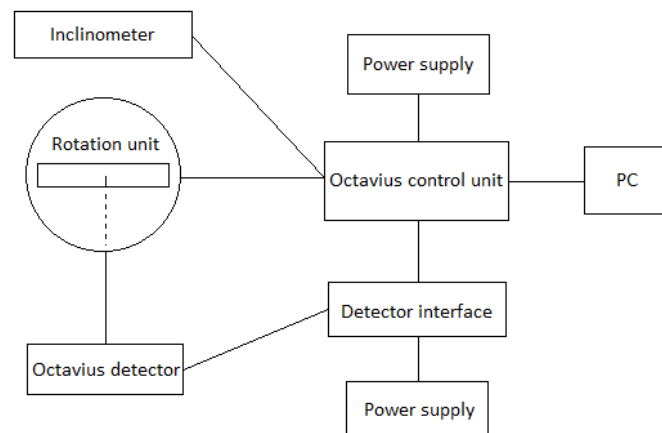


Figure 2.8: Connections diagram for the Octavius 4D. The inclinometer sends information about the gantry angle to the Octavius control unit, which in turn communicates with the 4D phantom to enable rotation. Dose measures are registered by the Octavius detector, sent to the detector interface and eventually to the Octavius control unit. All the gathered information from the control unit is then sent to the PC.

2.2.3 VeriSoft

VeriSoft allows to compare the measured dose against the calculated dose imported as a DICOM file from the TPS both for 2D and 3D dose reconstruction over the entire phantom volume.

We used this software to compare dose distributions obtained from the Octavius (both 2D and 4D configuration) with the calculated plan. VeriSoft implements a gamma-evaluation method to assess the pass rate for each point of the dose distribution, allowing fast dose verification. The implemented algorithm for 3D dose reconstruction is illustrated in the flow-chart below (Figure 2.9)

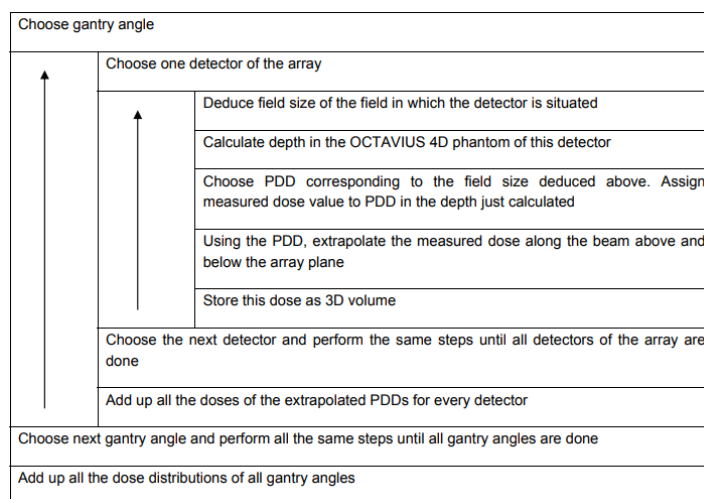


Figure 2.9: Algorithm implemented by the Verisoft software for 3D dose reconstruction [19]

Given a gantry angle, for any one detector of the array the field size is deduced and the depth in the Octavius 4D phantom is calculated. The PDD (Percentage Depth Dose, the absorbed dose deposited by the beam into the phantom at a certain depth over the maximum dose) corresponding to the geometry described above is calculated, then the extrapolated measured dose is calculated above and below the plane of the detector array. The dose distribution just obtained is stored as a 3D volume.

2.3 Film dosimetry with GafChromic EBT3

Radiochromic films such as Gafchromic EBT3 are designed for the measurement of absorbed doses of ionizing radiation, representing a useful tool for dose verification of modulated treatment plans and general quality assurance of TPS and linear accelerators. EBT3 films provide several characteristics that make them suitable for clinical QA routine: high spatial resolution, weak energy dependence and near-tissue equivalence. Moreover, they are self-developing, thus avoiding practical difficulties related to post-exposure treatments, and particularly suited for measures in the high-energy range. The range of absorbed doses in which they best perform is from 0.2 Gy to 10 Gy, this makes them suitable for applications in VMAT plans.

The experimental setup for radiochromic film dosimetry is composed of both the films and an RGB film scanner, the former being the detector with which ionizing radiation interact, the latter the digitalizing system that reads the detector's output for the actual dose evaluation. After 24h from irradiation, EBT3 can be scanned and the resulting tiff image is analyzed thanks to the dedicated software FilmQA Pro.

2.3.1 EBT3 films

EBT3 films are distributed in the standard size 8"x10" and boxed in packages of 25 sheets. Films are separated from one another by a piece of paper, and they are stored in a black envelope. It is recommended to keep the non-exposed sheets repaired from sunlight and at room temperature (20°C - 25°C). Nevertheless they can be handled under artificial light without noticeable effects. We used the whole sheet for our measures, but cutting smaller pieces is allowed, as long as it is kept the same orientation for every piece.

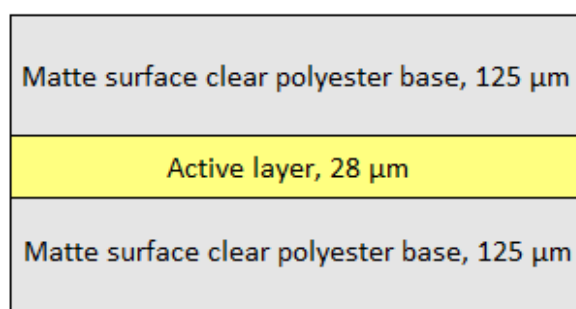


Figure 2.10: GafChromic EBT3 structure

The structure of EBT3 film is shown in Figure 2.10. They are made of three layers: the active layer, nominally 28 μm thick, surrounded by two 125 μm matte-polyester substrates. The active layer contains the active component, a marker dye, stabilizers

and other components to give the film its (almost) energy independent response. The thickness of the active layer will vary slightly between different production lots, as a consequence it is recommended that films for calibration and measures come from the same lot number. The polyester layers are designed to protect the inner active layer, making these films suitable for water immersion. Taking notes with a marker is also allowed. Moreover, the symmetrical structure allows for side-independent measures.

Property	GAFChromic™ EBT3 Film
Configuration	Active layer (28 μm) sandwiched between 125 μm matte-surface polyester substrates
Size	8" x 10", other sizes available upon request
Dynamic Dose Range	0.1 to 20 Gy
Energy dependency	<5% difference in net optical density when exposed at 100 keV and 18 MeV
Dose fractionation response	<5% difference in net optical density for a single 25 Gy dose and five cumulative 5 Gy doses at 30 min. intervals
Dose rate response	<5% difference in net optical density for 10 Gy exposures at rates of 3.4 Gy/min. and 0.034 Gy/min.
Stability in light	< 5×10^{-3} change in optical density per 1000 lux-day
Stability in dark (pre-exposure stability)	< 5×10^{-4} optical density change/day at 23 °C and < 2×10^{-4} density change/day refrigerated
Uniformity	Better than $\pm 3\%$ in sensitometric response from mean; dose uniformity better than $\pm 2\%$ with FilmQAPro and triple-channel dosimetry

Figure 2.11: GafChromic EBT3 specifications [1]

When unexposed, EBT3 are yellow, then when the active component is irradiated, it reacts to form a blue colored polymer.

2.3.2 Scanner

Since Gafchromic radiochromic films produce colored images when exposed to radiation, multichannel flatbed scanners perform better than white-light scanners.

Radiochromic films provide a different response for each color channel, and this is particularly because the slopes of color response vs dose response are different for each channel. An RGB scanner with a multichannel approach can separate the color response into a dose-dependent part and a dose-independent part. Up to 8 Gy the red color channel provides the most sensitive response for EBT3 films (Figure 2.12).

Higher doses from 8 Gy and over 40 Gy are covered by the green channel. The blue channel instead provides the dose-independent signal for automatic film uniformity enhancement through a special marker dye in the films active layer. The dose-independent

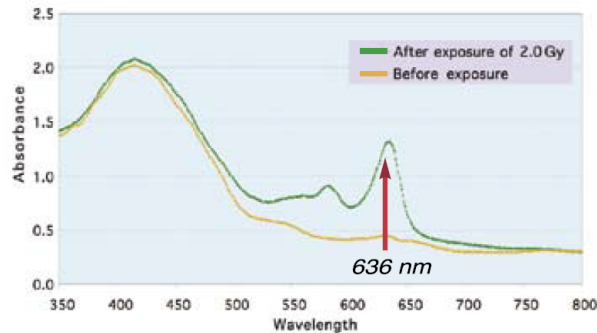


Figure 2.12: Absorption spectra of EBT3 before and after irradiation. The peak at 636 nm suggests that a more efficient dose response can be obtained analyzing the red color channel [1]

signal in fact includes information related to thickness, or other response differences in the film coating as well as to scanner artifacts, including noise, and to some effects caused by dust particles on the scanner. Having separated the dose-independent part of the scan information, the remaining dose-dependent information constituting the dose map has higher fidelity and becomes more useful to the user for the purposes of the dosimetry.

As for the acquisition process, under the glass surface on which films are layed, an optical train moves transporting the optical elements.

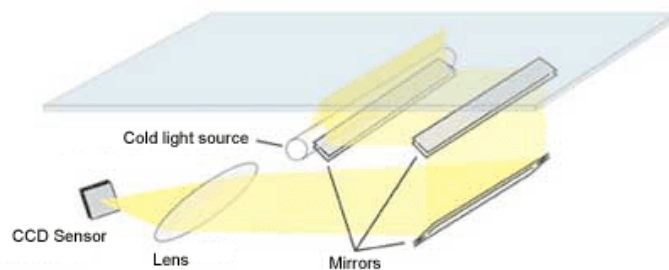


Figure 2.13: Functioning principle of a CCD scanner

As illustrated in Figure 2.13, a fluorescent lamp illuminates the film on the glass surface, and the resulting reflection is projected and focused by means of mirrors and a lens on the CCD (Charged Couple Device) sensor, equipped with filters for the three color channels, which in turn converts the luminous signal into electric pulses. For every scanned line, the CCD generates an analogic potential difference proportional to the incident light on the device. Eventually, this is sent to an ADC (Analog to Digital Converter) to obtain

digital data representing color levels.

For our acquisitions we used the recommended Epson Expression 10000XL flatbed color scanner. Table 2.1 shows the most important technical details.

Manufacturer	Epson
Model	Expression 10000XL
Max Document Size	12.2 in x 17.2 in
Supported Document Type	Transparencies, plain paper, slides, film
Optical Resolution	2400 dpi x 4800 dpi
Type	flatbed scanner
Scanner Speed Details	16 ms/line - color - 2400 dpi
Scan Element Type	CCD
Color Depth	48-bit color
Lamp / Light Source Type	xenon gas fluorescent lamp

Table 2.1: Epson Expression 10000XL specifications.

Optical resolution is defined as the number of dots per inch the scanner lens can detect. In particular, the number of photosensible cells of the CCD affects the horizontal resolution, 2400 dpi (the most important one, usually reported first), while the micro-movements of the CCD detector affect the vertical resolution, 3200 dpi.

Color depth represents the maximum number of colors the scanner can detect. This is expressed by means of bits: a 48-bit color scanner can detect 2^{16} colors for each channel, providing $2^{16} \times 2^{16} \times 2^{16}$ colors in total.

Flatbed scanners used for radiochromic film measurement are affected by a lateral scan artifact (LRA) that causes film density values to increase as the lateral distance from the scan axis increases. Generally, films scanned away from the center location exhibit a greater optical density and thus a higher calculated dose. While the effect is relatively small at low doses (<100 cGy) and positions within about 57 cm of the scan axis, it can create a significant overestimate of higher doses, particularly as film position approaches the lateral edges of the scan area [17].

The major cause for LRA is the polarization of light transmitted by the film and its following interaction with the mirrors in the optical train of the scanner. When the film is irradiated, the active component in the film polymerizes forming a colored polymer that polarizes transmitted light. At the lateral center of the scan area, incident rays are normal to the plane of the mirrors, but the angle of incidence increases as the distance from the center increases. As the rays transmitted by the film pass through the opti-

cal system, the reflectivity of the mirrors is influenced by the angle of incidence of the polarized light. As a consequence, for films with the same transmission placed at the lateral center and side of the scanner, the detected signal will be greater at the center and diminish towards the side of the scanner.

A smaller effect, due to the geometry of the optical system in flatbed scanners, results in an increase in the path-length of light through the film towards the lateral edges of the scanner. By the Beer-Lambert Law, this causes transmission to decrease with increasing distance from the center of the scanner, reinforcing the effects caused by polarization.

2.3.3 FilmQA Pro

FilmQA Pro is the dedicated software for GafChromic EBT3 analysis. It provides tools for color-dose calibration considering all three color channels, giving more accurate results than a single-channel analysis, effectively extending the dynamic range of the film [17].

The scanned images of the films are acquired via the Epson Scan software, owned by the scanner's manufacturer. The first requested operation is to select a film for calibration. The calibration tool allows to match selected areas of the film to a dose value and then outputs the calibration curves for the three color channels. When a new film calibration is completed, the obtained curves can be saved as a "Calibration Case" and can be reloaded and applied to as many films as desired.

The "Treatment Case" drop down menu allows then to load the image of the irradiated film obtained from the actual treatment delivery. Several operations are allowed such as cropping, rotation and many filtering tools to correct eventual flaws. It is recommended to set the reference points previously marked on the film so allineation is carried out automatically.

Eventually, the "Dose to plan comparison" menu allows to load a tiff file of the calculated plan from the TPS to evaluate a comparison in terms of gamma value. It is crucial that the images overlap perfectly, so several tools, both manual and automatic, are designated to reach a perfect match.

Chapter 3

Methods for dose verification

When it comes to complex treatments such as VMAT plans, the TPS system provides an enormous amount of data: the introduction of intensity-modulated beams requires extensive verification in two and three dimensions. In addition, modulated plans need to be checked for every patient before the delivery. This leads to the introduction of new dosimetry systems to validate the plan, as the traditional point-to-point or few-point detector system is not effective anymore.

This work focuses on the comparison of the calculated treatment plan from the TPS with the measured dose map obtained by two means: the Octavius (2D-array and 4D) and GafChromic EBT3 radiochromic films. In addition, a comparison is made between the two dosimetry systems, aiming to test if radiocrhomic films show a better spatial resolution as expected for clinical quality assurance purposes.

We proceed by steps: at first we test the validity of our protocol for VMAT plans under 0° gantry angle compared with the Octavius 2D-array and eventually added the rotational degree of freedom, using Octavius 4D as a benchmark.

In this chapter we illustrate the mathematical tools and describe the protocols implemented to obtain a quantitative dose evaluation for each of the steps described above.

3.1 The gamma evaluation method

Before we proceed with the description of the experimental setup and procedure for each step, it is necessary to introduce the mathematical tool that we use to evaluate the consistency of the measured dose map with respect to the treatment plan from the TPS.

The gamma evaluation method combines two parameters: the distance-to-agreement

(DTA) between measured and calculated dose distributions and a direct comparison of the two. A direct dose comparison is more effective in regions of low dose gradients, making an evaluation that is independent from spatial considerations. On the contrary, for regions with high gradients the DTA parameter is more meaningful.

A combined approach was proposed for bidimensional dose distributions for the first time in 1998 [14]. This considers a dose-difference criterion and a DTA criterion for each point of the dose distribution. This concept has been reviewed through time: the evaluated points are classified in different categories to reduce the amount of calculation time or to use linear interpolation for artifacts suppression. Moreover, the discretization of the gamma value is introduced, changing its continuous nature into a pass-fail decision for each point of the dose distribution [6]. As a result, we obtain a map of passed or failed points, but, on the other hand, the quantitative information on the numerical gamma value is lost. Later studies updated the evaluation method introducing new acceptance thresholds, based on the dose-gradient dependence and the presence of noise.

The interpretation of the gamma value matrix is of great importance, in fact, it is possible to analyze data statistically in order to understand whether a plan should be validated for treatment or not, in other words, it is necessary to define acceptance criteria.

Let D_m be the measured dose at coordinate r_m , D_c the calculated dose at coordinate r_c , ΔD_m the dose-difference tolerance criterion and Δd_m the DTA tolerance criterion, and given Equation 3.1

$$\Gamma(r_m, r_c) = \sqrt{\frac{r^2(r_m, r_c)}{\Delta d_m^2} + \frac{\delta^2(r_m, r_c)}{\Delta D_m^2}} \quad (3.1)$$

we define the gamma value as follows (Equation 3.2):

$$\gamma(r_m) = \min \Gamma(r_m, r_c) \forall r_c \quad (3.2)$$

with $\delta(r_m, r_c) = D_m - D_c$ and $r(r_m, r_c) = |r_m, r_c|$

We can also define another useful parameter: the gamma angle. This indicates the most influencing factor for the gamma value (the dose difference or the DTA) and is useful to interpret deviations. By definition, gamma angles of 0° are defined on the dose-difference axis, and those between $\frac{\pi}{4}$ and $\frac{\pi}{2}$ show a DTA criteria dominance. The angle is calculated with the absolute values of dose-difference and distance-difference so that the angle always ranges from 0 to $\frac{\pi}{2}$.

The parameters cited above are illustrated in Figure 3.1:

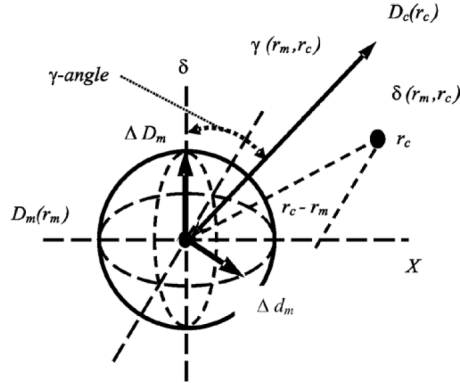


Figure 3.1: Definition of the gamma value and gamma angle

The acceptance threshold for gamma evaluation expressed as numerical values changes depending on a variety of factors concerning the single plan.

The numerical values generally accepted for VMAT treatments depend on the type of the fields implemented. Typically, for open, regular and conformation fields it is accepted a discrepancy of 2% in the in-depth dose difference for low gradient regions and 2mm for the DTA in high gradient regions. Concerning the discrepancy in the dose difference and DTA along the dose profile, 3% and 3mm are accepted respectively.

As for modulated VMAT plans, the tolerance for bidimensional dose distributions is generally set to the 3%-3mm limit.

3.2 Dose verification with the Octavius system

As introduced in the previous chapter, we employ the Octavius phantom with two different configurations: the bidimensional array only, to measure dose maps on the isocenter plane, and the Octavius 4D phantom that rotates the detector synchronously with the gantry, so that it is always perpendicular to the beam, thus eliminating any angular dependence of the detector response. The latter can provide a 4D reconstruction of the delivered dose, thus being very useful for VMAT treatment plans.

3.2.1 Two dimensional array

To test the performance in terms of gamma value with the 2D configuration we deliver at first a flat field of 10.5x10.5 cm² at 10 MV for calibration, then we deliver a modulated VMAT field at 10 MV clinically employed for prostate cancer treatment.

The diagram of the experimental setup we use is illustrated in Figure 3.2:

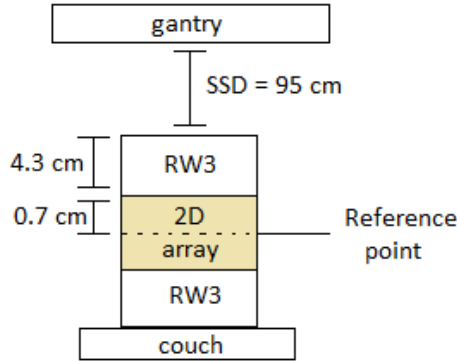


Figure 3.2: Experimental setup for the 2D-array plan measurement (not to scale). A 4.3 cm layer of solid water is placed over the surface of the Octavius as the measuring point of the chambers is 0.75 cm below the surface of the phantom, so that the measuring point is located 5 cm below the RW3 slabs, making it easier to place the radiochromic film in the same position for later measurements.

The VMAT plan is first calculated by Monaco on the CT image of the 2D-array phantom we use for measures. In this first trial, the plan is calculated without rotation: the gantry position is fixed at 0° , thus the field modulation we obtain is only planar and simpler than a 3D dose distribution.

Before we start the data acquisition, we irradiate 5000 MU (Monitor Unit). The actual dose value corresponding to a monitor unit depends on the calibration of the ionization chamber in the linac's treatment head. Based on our calibration, we define 100 MU to be the dose value read under 10 cm of solid water (positioned at $SSD = 90$ cm) when 100 cGy are irradiated as an uniform flat field of 10×10 cm² on the isocenter plane ($SSD = 100$ cm). The preliminar irradiation is needed to warm up the electronic components of the Octavius; after this we don't deliver any radiation for about a minute so that the Octavius can record the background to subtract it automatically from the actual dose measure.

We analyze the data we obtain with the dedicated software VeriSoft, mentioned in the previous chapter. VeriSoft can import the calculated dose map from the TPS and compare it with the measured dose map. The evaluation is made in terms of gamma value after a few corrections for temperature, pressure and beam quality are calculated. In particular, air density corrections are needed as the Octavius detector is a vented ionization chamber array.

We can insert environmental parameters (temperature, pressure) manually to calculate

the k_{TP} factor for air density. The k_{TP} is calculated from equation 3.3:

$$k_{TP} = \frac{(273.2 + T) \cdot P_0}{(273.2 + T_0) \cdot P} \quad (3.3)$$

where T is the temperature in the measuring volume ($^{\circ}\text{C}$), P is the air pressure at the measuring site (hPa), T_0 is the reference temperature (20°C or 22°C) and P_0 the reference air pressure (1013.25 hPa).

We can optionally indicate a k_{energy} factor to take into account corrections for beam quality. Eventually, an additional k_{user} factor can be added for other corrections. The final correction parameter can be expressed as the product of these three parameters:

$$k = k_{TP} \cdot k_{energy} \cdot k_{user} \quad (3.4)$$

Another approach is the cross calibration. This allows to insert an expected dose value for the reference measurement of the center chamber and irradiate the reference field afterwards to get the “real” measurement. The comparison between the expected and measured dose value will serve for determining the calibration factor.

We evaluated both methods and chose for the cross validation, inserting as expected dose value the one given by the TPS. This choice is supported by the fact that the dose estimated by the TPS is in good agreement with the measure performed by a single ionization chamber, thus we conclude it can offer a reliable prediction.

After the calibration factor is calculated we proceed by irradiating the modulated field. The gamma evaluation of the dose maps we obtained is discussed in the results chapter.

3.2.2 Octavius 4D phantom

Employing the dedicated 4D phantom it is possible to reproduce a 4D dose distribution. We can choose to record the integral of the dose irradiated on each chamber when the phantom rotation is blocked, or the dose assigned to each chamber calculated from the beam projection while the phantom rotates with the gantry. Our measures are carried out in both the arrangements.

Before irradiation, we have to fix the coordinate system: the phantom provides three crosses that should match with the laser system in the room in order to set the phantom to the isocenter. Then we connect the phantom with the inclinometer thanks to the bluetooth device (see materials chapter) and let the Octavius rotate to the left and then to the right to calibrate for rotation. The experimental setup is shown in Figure 3.3.

As for the dose calibration factor, after blocking the phantom rotation, we irradiate a uniform 500 MU field to warm up the system, then wait about 60 seconds for the background recording and finally proceed with the calibration following the same procedure as the 2D configuration. For this purpose, we irradiate a $10 \times 10 \text{ cm}^2$ uniform field and perform a cross calibration.

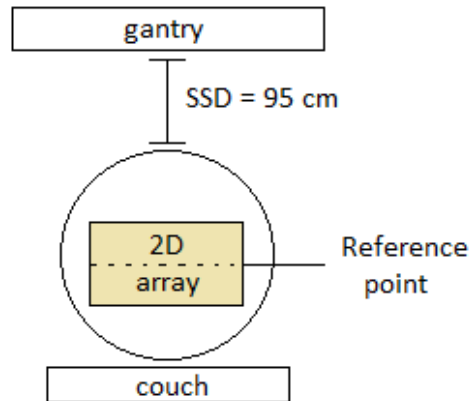


Figure 3.3: Experimental setup for the 4D measurement (not to scale). The 2D-array is located into the dedicated socket of the Octavius to allow for rotation.

The calculated plan we irradiate this time includes the rotation of the gantry, as done for real VMAT treatment plans. The first measurement we perform is carried out with Octavius rotation, the second without rotation (the calculated plan is the same in both cases). The VeriSoft software allows to save dose values considering or not the rotation, so that we can later compare the data with those obtained employing films in the same configuration. The dose maps we obtain are discussed in the results chapter.

3.3 Dose verification with EBT3 films

3.3.1 Dose calibration

It is necessary to associate a dose value to red, green and blue channel levels of the irradiated films in order to get a dose response and make comparisons with other dose measurements. This is a preliminar procedure that should be carried out for every film set.

The experimental setup is illustrated in Figure 3.4. RW3 slab phantoms are made of a water-equivalent material, RW3 (98% polystyrene + 2% TiO_2). We place them below the film and chamber to provide for backscattering and over the film to measure the dose at a certain depth (in this case 5 cm). RW3 slabs are provided with different thickness ranging from 1 mm to 10 mm and thickness tolerance of ± 0.1 mm; a special slab is also included to hold the chamber. The whole system is placed so that the Source-Surface Distance (SSD) is equal to 95 cm.

We irradiate the same film with fields of 0, 50, 100, 200, 300, 500, 700, 900 and 1100 MU respectively and measure the absolute dose value for each field with the chamber. Moreover, every erogated field has a different geometry, so that from their superposition we obtain the sequence described above in eight rectangles with dimension $5 \times 4 \text{ cm}^2$ (Figure 3.5).

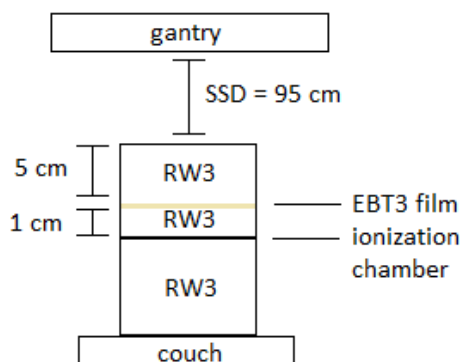


Figure 3.4: Experimental setup for film calibration (not to scale). A Farmer type ionization chamber is located 1 cm below the film to measure an absolute dose value.

The FilmQAPro software extracts calibration curves for each color channel automatically analyzing the RGB levels of selected areas from a TIFF image (see Figure 3.5) and matching this information with dose values inserted manually after corrections are applied for air density and position (the latter is needed to read the expected dose value at the same depth as the film).

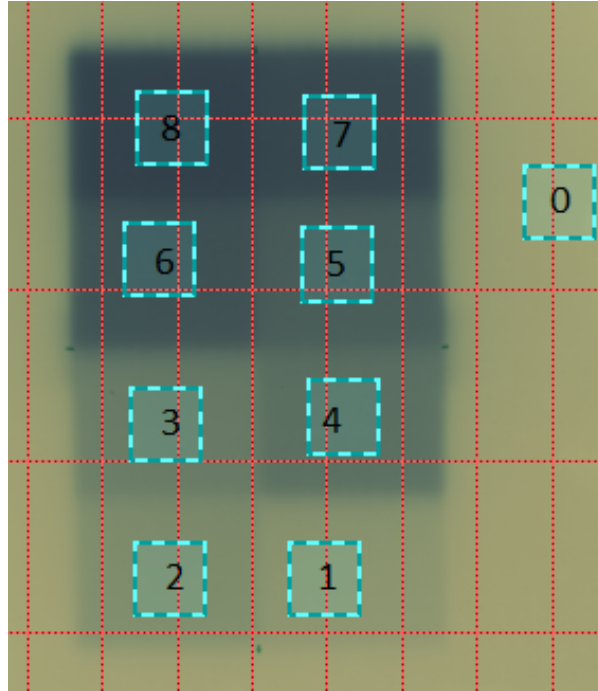


Figure 3.5: Irradiated film for calibration. Numbers 1 to 8 represent areas with increasing dose, 0 represents an area with no dose. The ionization chamber, as well as the isocenter, is placed at the center of the rectangle with the 6 label.

We selected the central areas of each dose zone as recommended, in fact that position provides a more uniform irradiation and thus, as a consequence, it is possible to perform a better calibration.

To calibrate films, the software is equipped with several rational functions, obtained from polynomial functions. In the past, interpolation was obtained with polynomial functions only, but this more recent approach can reduce calibration errors and also the minimum number of needed points for interpolation, which is three. The default function for calibration is illustrated in equation 3.5:

$$f(D) = \frac{a + b}{D - c} \quad (3.5)$$

where D is the dose value, $f(D)$ the color level and a , b and c depend on the function type.

Figure 3.6 illustrates the results we obtained:

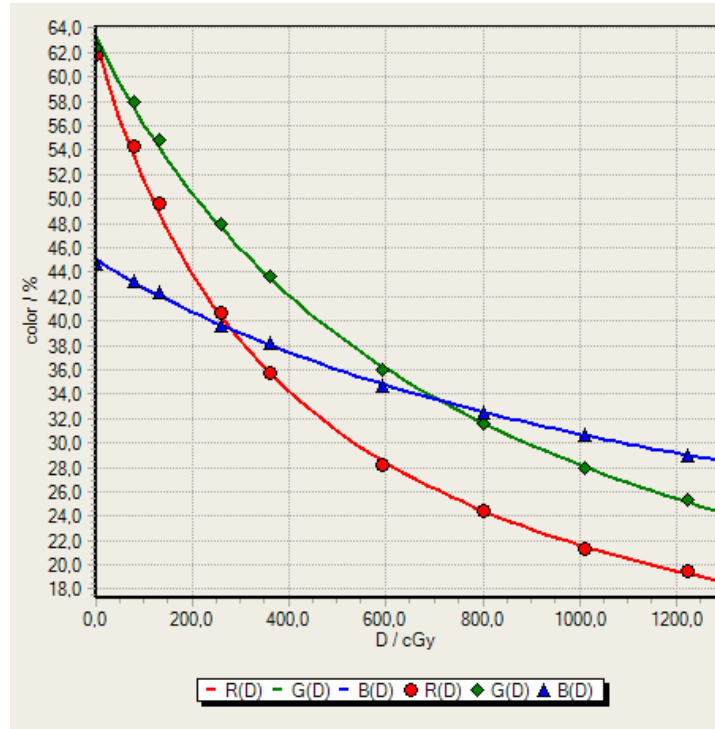


Figure 3.6: Calibration curves for the three color channels.

3.3.2 2D plan

In order to compare the results we obtain from the 2D-array and the film, we have to place the latter in the same position as the array measuring point. The diagram of the experimental setup is illustrated in Figure 3.7.

Before irradiation we report on the film four references to pinpoint the isocenter position and we mark the film orientation with respect to the gantry. This is needed for later software elaboration, as explained in the scanning protocol appendix.

After irradiation, we wait for at least 24 hours before scanning the film, so the self-development is fully completed.

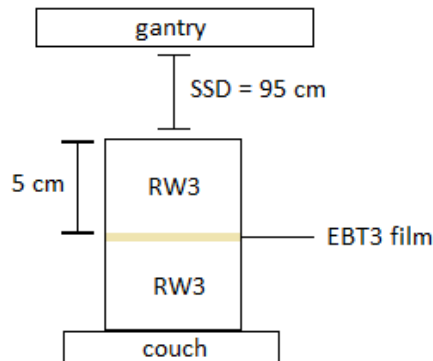


Figure 3.7: Experimental setup for the 2D plan measurement with film (not to scale). A 5 cm layer of solid water is placed over the surface of the film. The film is itself placed over another layer of solid water to prevent backscattering effects.

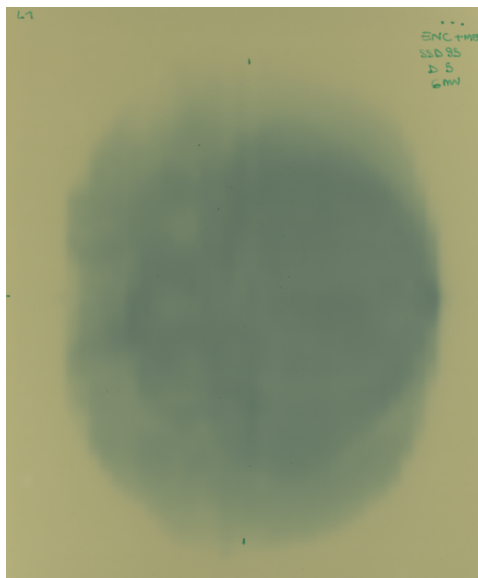


Figure 3.8: Irradiated film for brain cancer treatment

3.3.3 4D plan

As the 2D arrangement, we want to place the film in the same position as the measuring point of the 4D Octavius. Thus we place the film between two layers of solid water and insert the whole composition into the 2D-array location in the 4D Octavius. A more detailed diagram is illustrated in Figure 3.9 and 3.10.

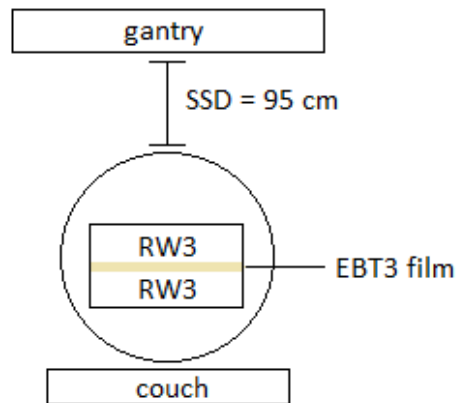


Figure 3.9: Experimental setup for the 4D plan measurement with film (not to scale). The film is placed between two layers of solid water.

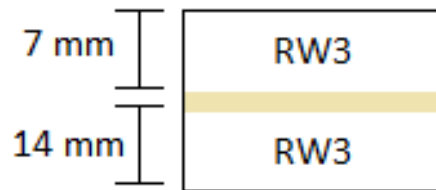


Figure 3.10: Detail of the experimental setup

As explained in section 3.2.2, we first block the 4D phantom and then start the acquisition with rotation also.

Chapter 4

Results and discussion

We report here the results obtained for each experimental setup described in the previous chapter. In particular, dose maps are compared in terms of gamma value with both VeriSoft and FilmQA Pro software and a passing rate value is given in order to assess the comparison quantitatively.

4.1 Comparison of 2D dose maps

This section focuses on dose map comparisons obtained with both EBT3 films and the 2D array with the configuration described in section 3.2.1 and 3.3.2: the gantry is blocked so the VMAT plan is irradiated without any rotation.

4.1.1 Uniform flat field

The preliminar acquisition of a 10.5×10.5 cm² uniform flat field is illustrated in Figure 4.1. The VeriSoft interface displays on the top left the dose map corresponding to the 2D array configuration and the bottom left is the dose map calculated from the TPS. A passing rate of 100% is reached within 3mm DTA and 3% dose difference. The chart on the bottom right shows the distribution in false color of the gamma value over the whole dose map. The green color, corresponding to a gamma value of 0, indicates a perfect match of the two dose distributions.

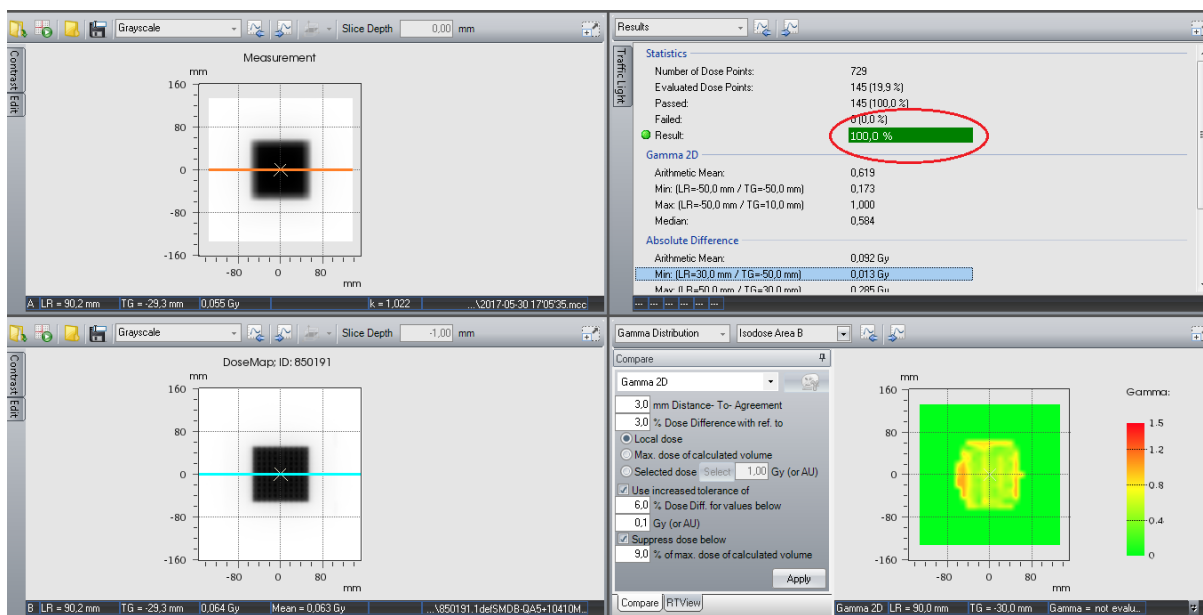


Figure 4.1: Comparison between the calculated dose map (TPS) and the measured dose map (bidimensional array)

Figure 4.2 shows the horizontal profile of the calculated dose map and the profile of the measured map extrapolated in the same position.

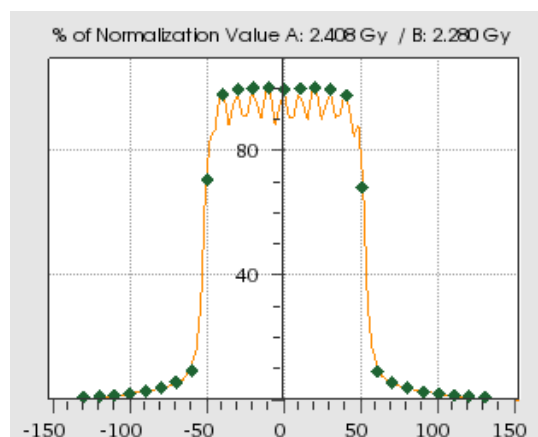


Figure 4.2: Horizontal profiles of the measured (green dots) and calculated (orange line) profile

It can be noted at first glance that the measured profile from the 2D array is a set of discrete points, as a result of the spatial distance (1 cm) between the measuring points of the chambers in the 2D array.

The comparison between the calculated dose map and the measured one with EBT3 is illustrated in Figure 4.3.

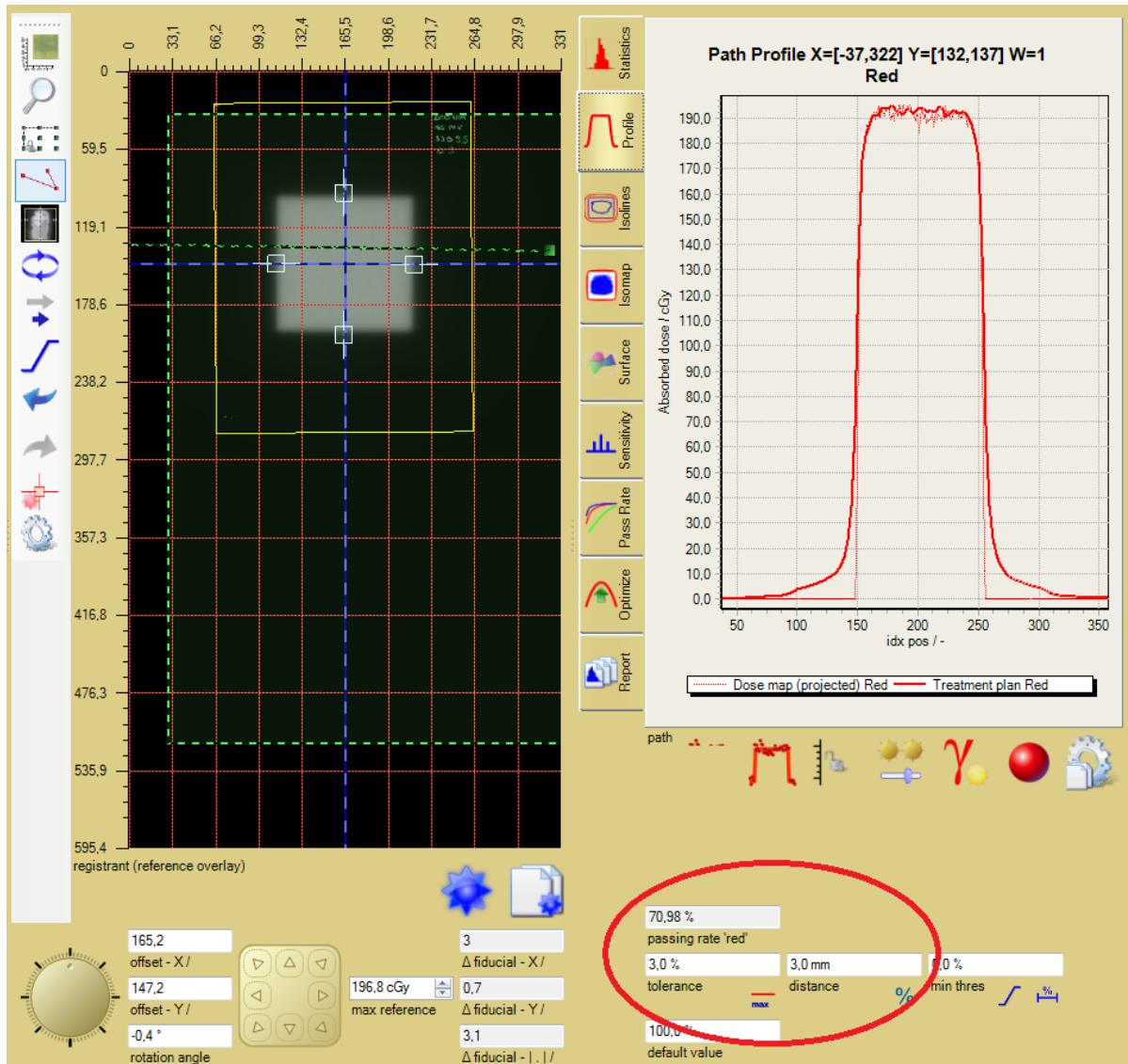


Figure 4.3: Comparison between the calculated dose map (TPS) and the measured dose map (film).

The film can provide a continuous response, as highlighted by the profile on the right of Figure 4.3, where the thick red line is extrapolated from the calculated dose map and the thin red line represents the corresponding measured dose profile. The passing rate within 3mm/3% is here 72%.

Eventually, a direct comparison between the measured dose map from the film and the 2D array is given (Figure 4.4).

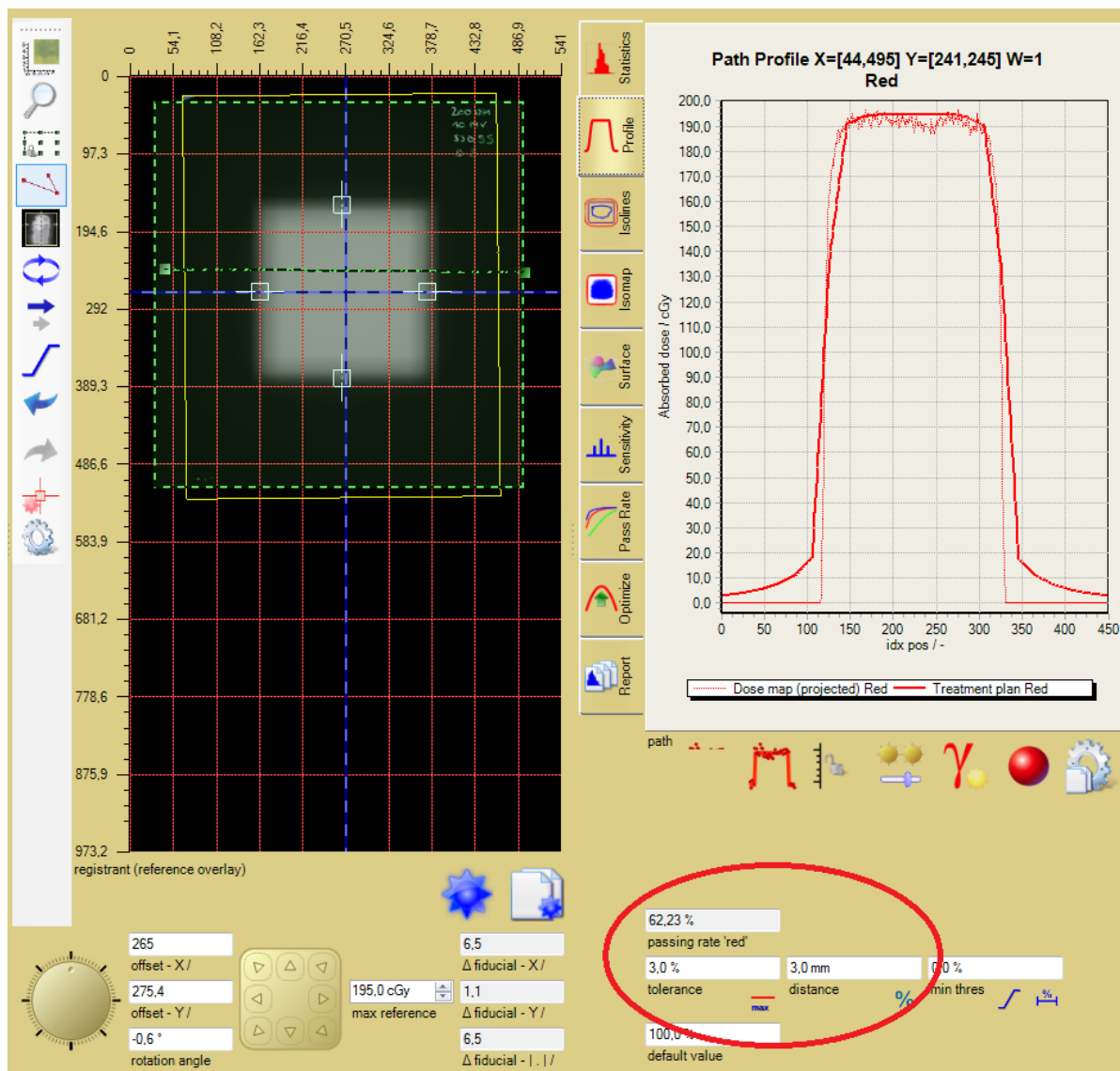


Figure 4.4: Comparison between the measured dose map from both the film and the 2D array

While the film profile (thin line) is entirely determined by the irradiation, the 2D array profile is an interpolation of a few experimental points (see Figure 4.2), providing a less informative response. The passing rate within 3mm/3% is 62%.

4.1.2 Modulated plans

We report the results obtained for two real clinical cases we irradiated with a bidimensional configuration: a prostate treatment and an encephalon treatment with metastasis. The first one has a simpler beam geometry while the second one is highly modulated. Results in terms of gamma value are provided for both cases.

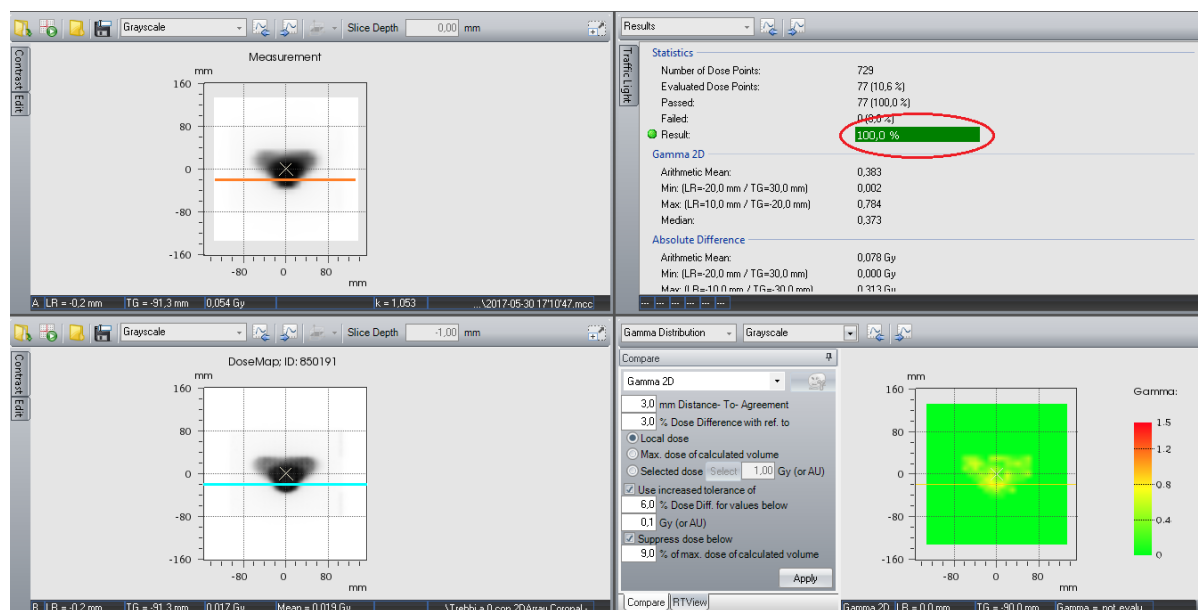


Figure 4.5: Comparison between the calculated (TPS) and measured (2D array) dose maps for the prostate case

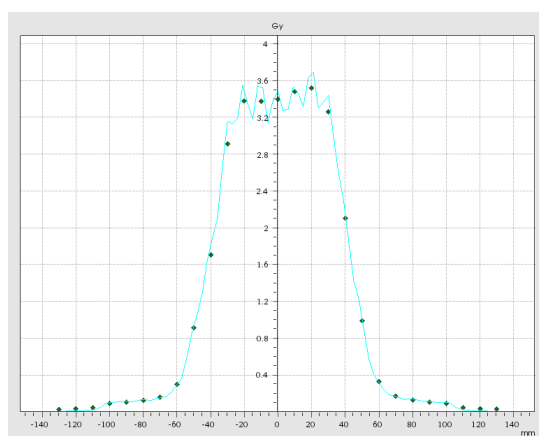


Figure 4.6: Dose profiles comparing the TPS (blue curve) and the 2D array (green dots) for the prostate case

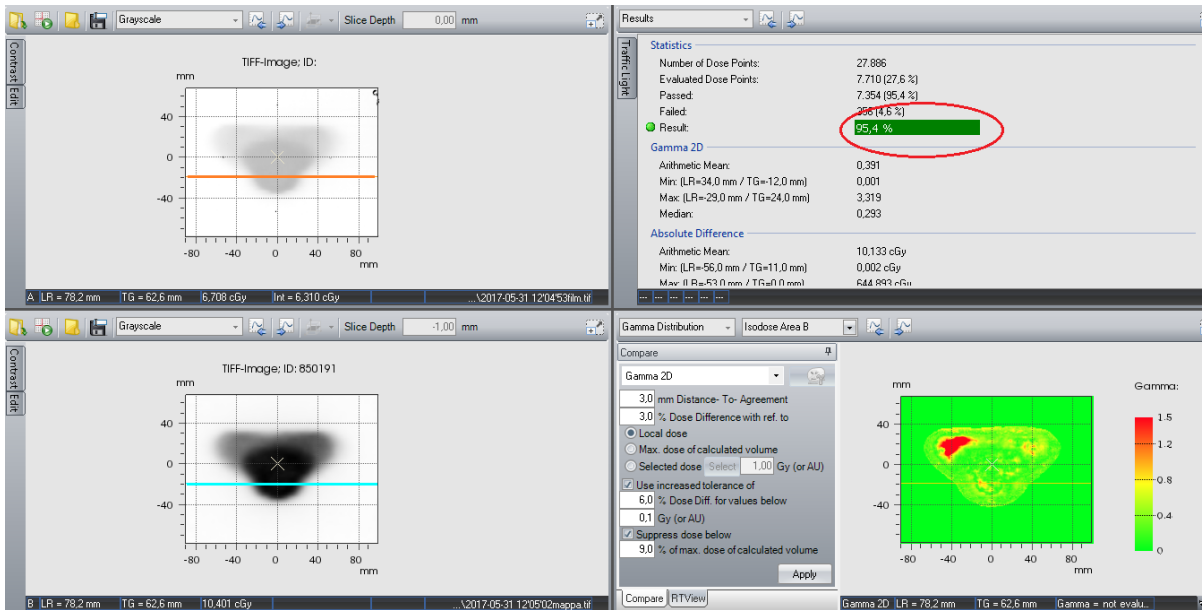


Figure 4.7: Comparison between the calculated (TPS) and measured (film) dose maps for the prostate case

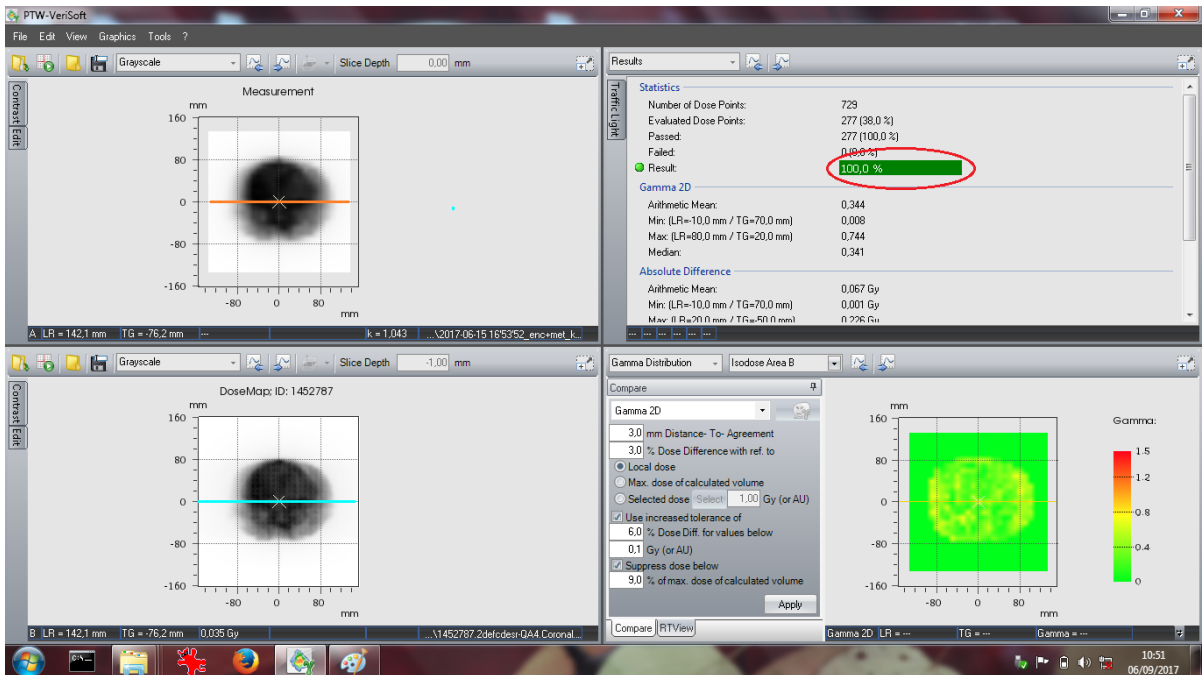


Figure 4.8: Comparison between the calculated (TPS) and measured (2D array) dose maps for the encephalon case

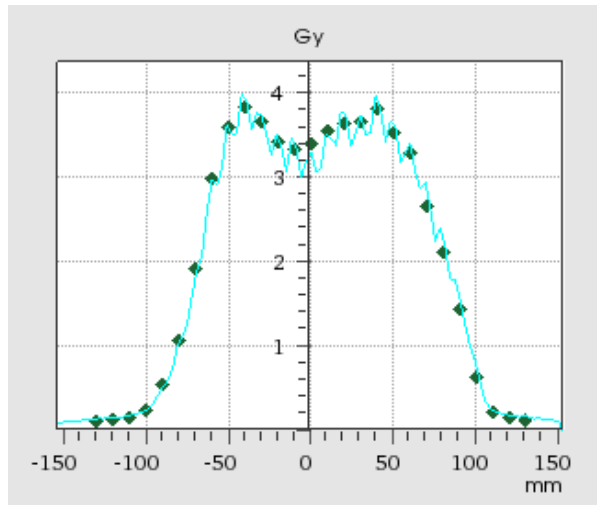


Figure 4.9: Dose profiles comparing the TPS (blue curve) and the 2D array (green dots) for the encephalon case

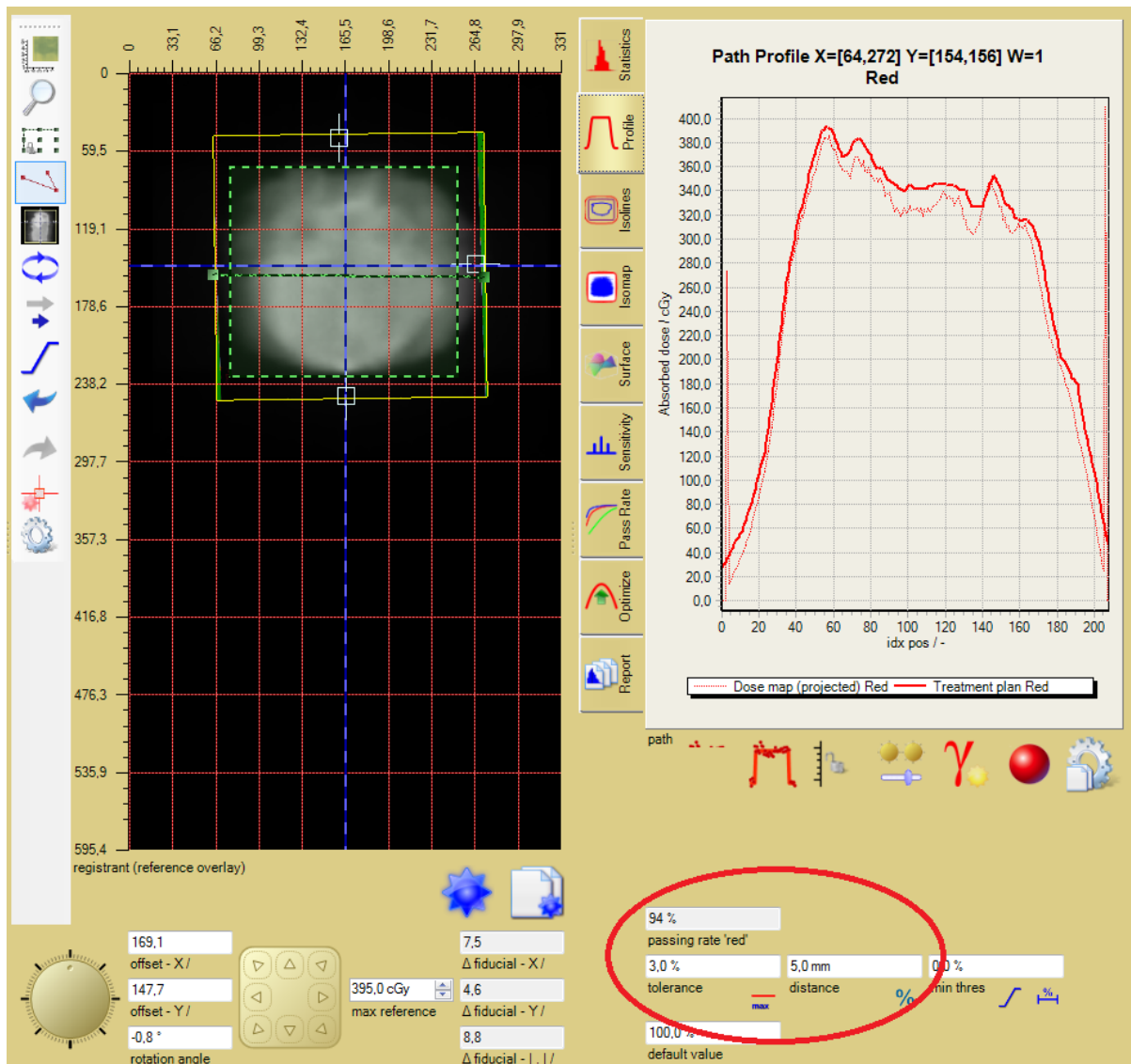


Figure 4.10: Comparison between the calculated (TPS) and measured (film) dose maps for the encephalon case. The film profile is represented by the thin line and the TPS profile is represented by the thick line.

The 2D array provides a perfect response in both cases, with a 100% passing rate within 3mm/3%. The film is suboptimal for the simpler prostate case (95.4 within 3mm/3%) but when it comes to the encephalon the response is good within a larger margin (5mm/3%), nonetheless its dose profile is in good agreement with the dose profile calculated from the TPS.

4.2 Comparison of 4D dose maps

In this section we report the results of irradiation of complete VMAT plans, that is with the gantry rotation. At first we blocked the Octavius system rotation and eventually added it.

4.2.1 Irradiation without Octavius system rotation

The following results are obtained from irradiation of a real clinical plan for the treatment of a head and neck tumor with reference to the configuration illustrated in section 3.3.3.

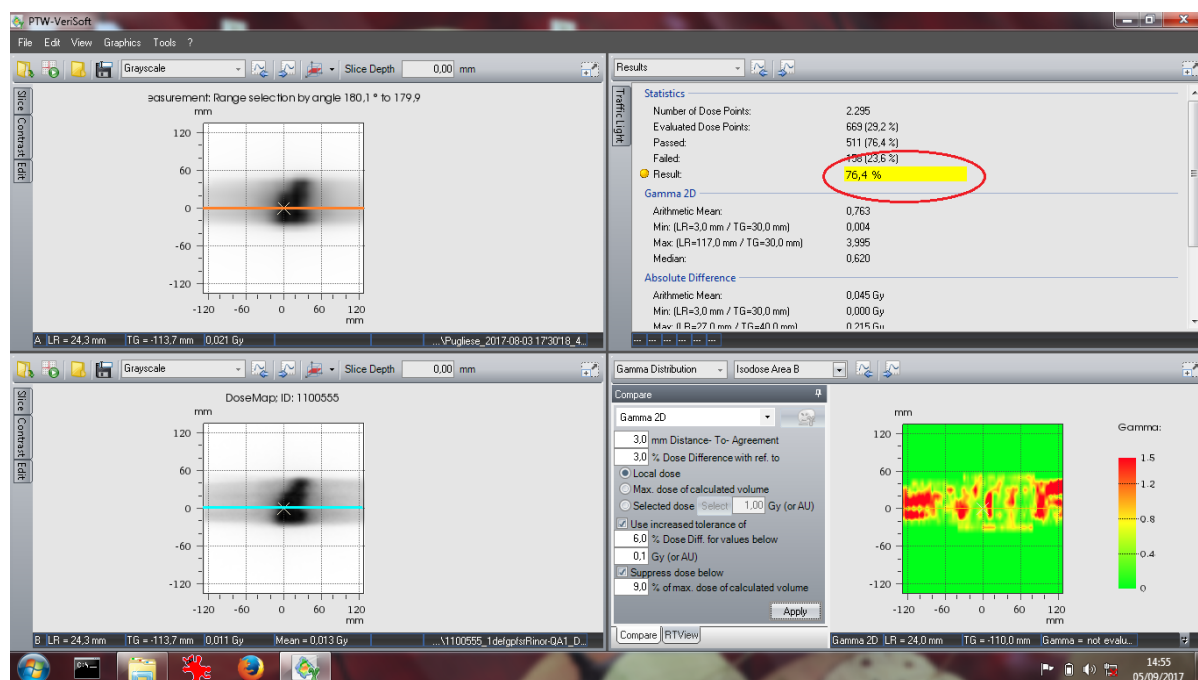


Figure 4.11: Comparison between the calculated (TPS) and measured (Octavius system) dose maps for the treatment of a head and neck tumor.

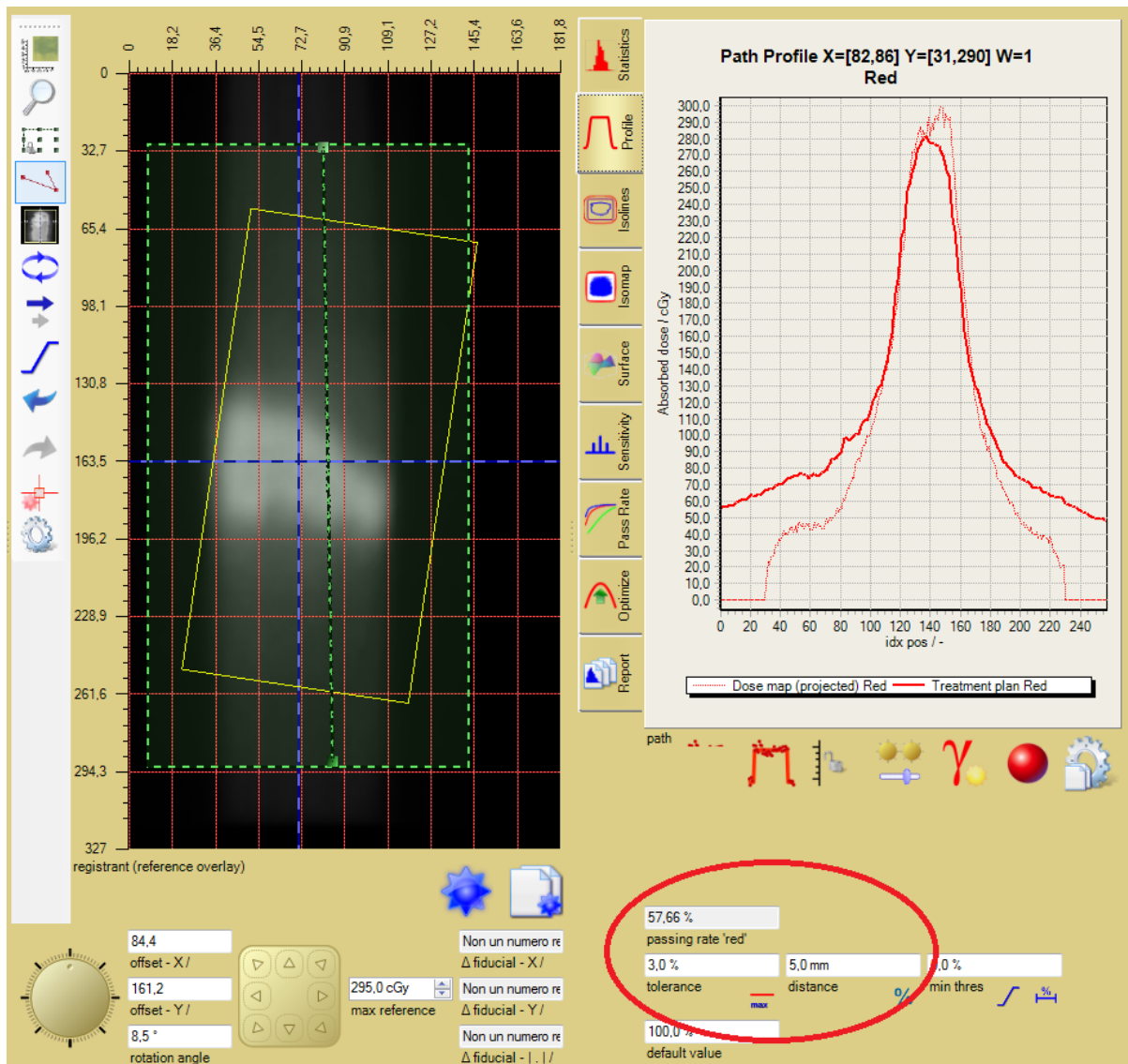


Figure 4.12: Comparison between the calculated (TPS) and measured (film) dose maps for the treatment of a head and neck tumor.

The octavius system response is not good for this configuration, the passing rate within a 3mm/3% limit is 76%, far from an acceptable result for clinical implementation. As for the film, the response within a wider margin (5mm/3%) is still unsatisfying: the passing rate is only 58%.

4.2.2 Irradiation with Octavius system rotation

This last configuration is the one usually implemented for clinical QA. The results displayed here are referred to the configuration described in section 3.3.3, this time allowing the rotation of the Octavius system. We report the clinical case of the encephalon already employed for irradiation in the bidimensional configuration.

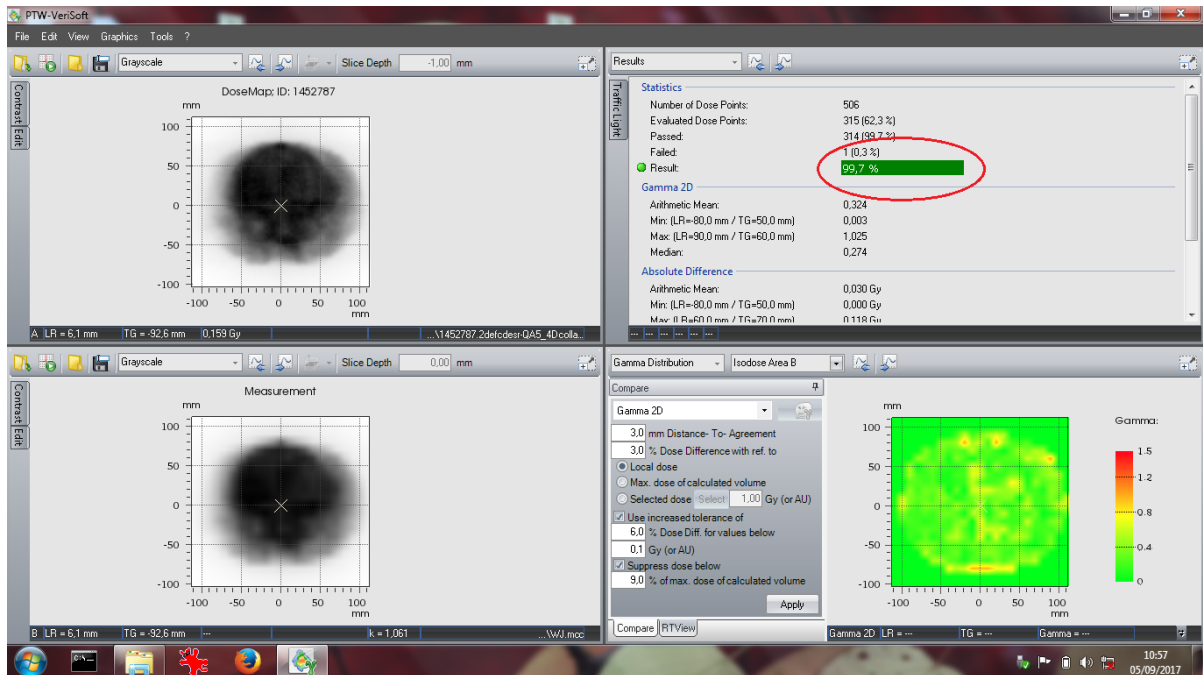


Figure 4.13: Comparison between the calculated (TPS) and measured (Octavius system) dose maps for the treatment of an encephalon tumor.

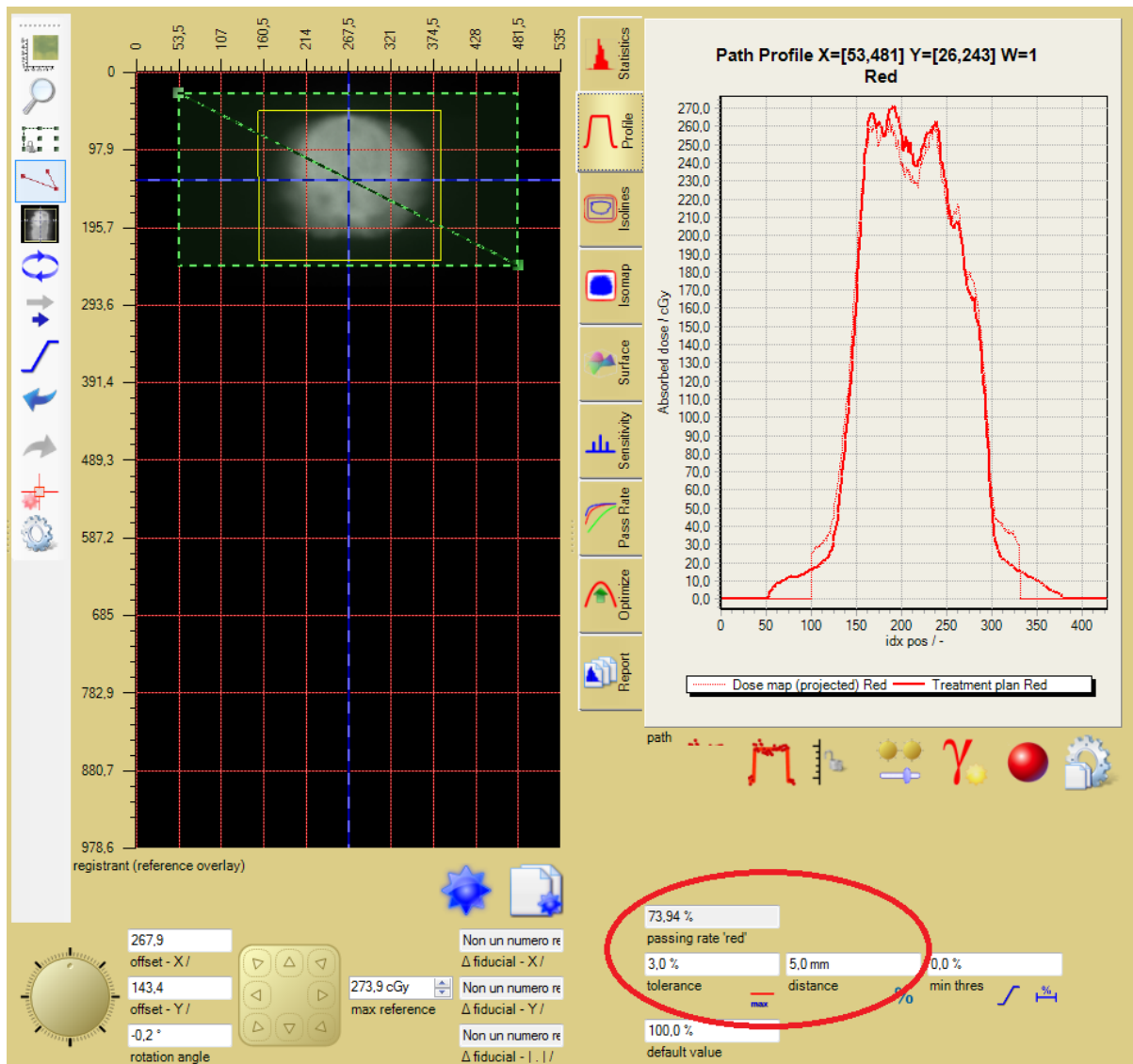


Figure 4.14: Comparison between the calculated (TPS) and measured (film) dose maps for the treatment of an encephalon tumor.

As we expected, the response of the Octavius system is almost perfect with this configuration within the 3mm/3% limit, providing a passing rate of 99.7%. The film cannot perform as well as the Octavius: within a wider margin of 5mm/3% the response is still unacceptable for clinical purposes, only providing a passing rate of 74%.

4.3 Discussion

A sequence of plans has been irradiated with both films and the Octavius in different configurations of overall increasing complexity, adding one degree of freedom at a time.

It is immediate to note that the Octavius system as a whole, that is both the 2D array only and the 4D system configuration, performs better than films, whatever the experimental configuration is, in terms of gamma evaluation. Several factors, concerning both the experimental procedure and especially the scanning process, contribute to the observed discrepancies as noise sources.

Concerning the experimental setups, the most important uncertainty is given by the inaccurate position of the film. As we fix the film with adhesive tape on a RW3 slab we cannot be sure that the whole film surface adheres to the phantom. Moreover, slabs are not perfectly regular, there are gaps between the layered slabs (this is well visible on the ct scan of the phantom). This effect gains much more importance when we employ the 4D configuration, firstly because we cannot fix the reference points on the film before irradiating, so later analysis is much more difficult, but most importantly because we cannot be sure that during the phantom rotation the film does not move from the position where we initially set it. This is especially because the film is inserted between a custom layer of solid water, but this does not perfectly fit in the 4D phantom like the 2D array does. Moreover, the exact depth of the film with respect to the isocenter plane is difficult to determine.

By comparison, the 2D array and the Octavius 4D system as well, are integrated dosimetry systems, providing a more accurate positioning and thus depth at which the effective dose measurement takes place.

The crucial point about dose evaluation with films is undoubtedly their elaboration, as it is firmly linked to the efficiency of the scanning process, thus a variety of factors can affect the outcome. Among these, for example, is the already mentioned LRA, the possibility that dust grains or other impurities deposite on the glass even if it has been cleaned, the imperfect adhesion of films to the glass and other nonuniformities closely related to the scanning functioning principle, i.e. the lamp is not well heated, the movements of the optic system are not precise. To some of the listed effects we could find a solution, i.e. stabilizing the temperature of the lamp by taking three scans without the film and preheating the scanner before acquisition, as suggested in [7]. We also have to consider that, unlike the Octavius system, films can only provide a relative dose evaluation and the needed calibration process is carried out by scanning the film, so it is affected by all the effects described above and will in turn have an influence on later measurements.

Eventually, even if the EBT3 model is less sensitive than older radiochromic films [1], the environment, i.e. the exposure to sunlight or other radiation sources, could still affect the measure.

Apart from the purely quantitative dose evaluation discussed above, we could appreciate a better response of films with respect to resolution, as was our purpose. Our first measurement, a flat field, can highlight this very well: the dose distribution calculated by the TPS has a very steep gradient, going from about 250 cGy to 0 cGy within 3 mm, so the resolution of the 2D array is not sufficient to accurately reconstruct the dose curve, as it can provide only one measuring point over the whole steep part of the curve (see Figure 4.2). Even if we observed that the film is not superior to the 2D array in terms of gamma evaluation, this simple case shows how it could be more informative in some situations, i.e. when we have to deliver a highly modulated plan and we need to make sure that OARs are saved. Dose profiles extrapolated from more complex plans show a good agreement of the TPS with the films response as well (see Figure 4.10 and 4.14), even if our results need to be improved for application in clinical QA. In fact, uncertainties about the film position with respect to the isocenter cannot be admitted, as well as gamma values below 95% within the 3mm/3% range.

As for the results reported in section 4.2.1, where the outcome is unacceptable for both the Octavius and films, it is worth noting that we decided to irradiate the plan with that particular configuration to test our procedure in a simpler situation with respect to the complete VMAT plan, but that setup has no clinical meaning, and the experimental equipment is not optimized to detect radiation with that geometry. The film is bidimensional so we do not know how a lateral irradiation affects our measure; in addition, avoiding the Octavius rotation we lose the independence of the chambers response with respect to the incident beams direction.

Conclusions and further developments

The purpose of this work was to assess the performance of GafChromic EBT3 films with respect to the currently implemented dosimetry system, Octavius 4D. Overall, we could observe that the ionization chambers based system provides a better response on the quantitative dose evaluation, but film dosimetry can provide a better resolution, which is crucial for highly modulated treatment plans such as VMAT.

Further developments consist in improving the accuracy of our experimental procedure, especially concerning the handling of films during irradiation and, above all, elaboration in order to make film dosimetry a reliable tool for dose verification, with a clinically acceptable response. Some suggestions could be, for example, covering the film with a plexiglas slab to make the film adhere to the scanner glass, thus improving the scanning procedure, the weakest link in the chain; in addition, image processing after scanning (i.e. averaging several images of the same irradiated film) could help in reducing the influence of scanning artifacts on the final outcome.

Appendix A

Scanning protocol

To perform film dosimetry we need to scan the films at least 24 hours after irradiation. As the scanner bed is wider than the film, to make it less susceptible to the lateral response artifact, we build a black paper mask in order to place the films centrally, where the scanner response is most homogeneous, and always in the same position.

Before the actual scanning two operations are needed: the scanner is switched on about half an hour before usage, in order to warm up the electronics, and then three “Preview” scans are performed without the film to warm up the light source. This assures a stable color temperature of the light source.

The scanner is equipped with the Epson Scan software, through which the whole scanning procedure is carried out. We set a few parameters before acquiring the image:

- **Professional mode:** allows activation of all possible selections
- **Film:** the preferred transparency mode is activated as opposed to reflection scanning
- **Positive film:** high/low response values correspond to light/dark areas on film
- **48-bit color:** activates three color channels with 16-bits/channel. 24-bit color (8-bits/channel) is unsuitable for accurate/precise film dosimetry
- **Resolution:** 75 dpi

It is important that all the image correction features are turned off, as the three-channel film dosimetry has to be performed on the raw color levels read by the detector. Filters would negatively affect the final dose response, only making the image more eye-appealing.

We first take a preview scan and crop the image to keep only our region of interest

(ROI), then acquire that ROI. The image file is then saved in .tiff format and is ready to be analyzed with the FilmQAPro software.

Bibliography

- [1] *GAFChromic EBT3 film specifications*, www.gafchromic.com.
- [2] EGA Aird and FT Farmer. The design of a thimble chamber for the farmer dosimeter. *Physics in medicine and biology*, 17(2):169, 1972.
- [3] B Allgaier, E Schüle, and J Würfel. Dose reconstruction in the octavius 4d phantom and in the patient without using dose information from the tps. *PTW White Pap*, page D913, 2013.
- [4] Judith Alvarez-Moret, Fabian Pohl, Oliver Koelbl, and Barbara Dobler. Evaluation of volumetric modulated arc therapy (vmat) with oncentra masterplan® for the treatment of head and neck cancer. *Radiation oncology*, 5(1):110, 2010.
- [5] VP Cosgrove, MDR Thomas, SJ Weston, MG Thompson, N Reynaert, CJ Evans, KJ Brown, Carlos De Wagter, DI Thwaites, and AP Warrington. Physical characterization of a new concept design of an Elekta radiation head with integrated 160-leaf multi-leaf collimator. *International Journal of Radiation Oncology* Biology* Physics*, 75(3):S722–S723, 2009.
- [6] Tom Depuydt, Ann Van Esch, and Dominique Pierre Huyskens. A quantitative evaluation of imrt dose distributions: refinement and clinical assessment of the gamma evaluation. *Radiotherapy and Oncology*, 62(3):309–319, 2002.
- [7] Slobodan Devic, Jan Seuntjens, Edwin Sham, Ervin B Podgorsak, C Ross Schmidlein, Assen S Kirov, and Christopher G Soares. Precise radiochromic film dosimetry using a flat-bed document scanner. *Medical physics*, 32(7):2245–2253, 2005.
- [8] Issam El Naqa, Piotr Pater, and Jan Seuntjens. Monte carlo role in radiobiological modelling of radiotherapy outcomes. *Physics in Medicine and Biology*, 57(11):R75, 2012.
- [9] Frank T Farmer. A sub-standard x-ray dose-meter. *The British journal of radiology*, 28(330):304–306, 1955.

- [10] Christian Fiandra, Umberto Ricardi, Riccardo Ragona, Silvia Anglesio, Francesca Romana Giglioli, Elisa Calamia, and Francesco Lucio. Clinical use of ebt model gafchromic film in radiotherapy. *Medical physics*, 33(11):4314–4319, 2006.
- [11] Mark A. Finlayson. *Agility and Integrity R3.1 Instructions for Use - Clinical Mode*. Elekta.
- [12] V Grégoire and TR Mackie. State of the art on dose prescription, reporting and recording in intensity-modulated radiation therapy (icru report no. 83). *Cancer/Radiothérapie*, 15(6):555–559, 2011.
- [13] Faiz M Khan. *The physics of radiation therapy*. Lippincott Williams & Wilkins, 2010.
- [14] Daniel A Low, William B Harms, Sasa Mutic, and James A Purdy. A technique for the quantitative evaluation of dose distributions. *Medical physics*, 25(5):656–661, 1998.
- [15] A Markus, S Broggi, and C De Wagter. Estro physics booklet nr. 9: Guidelines for the verification of imrt, 2008.
- [16] Martha M Matuszak, Di Yan, Inga Grills, and Alvaro Martinez. Clinical applications of volumetric modulated arc therapy. *International Journal of Radiation Oncology* Biology* Physics*, 77(2):608–616, 2010.
- [17] Andre Micke, David F Lewis, and Xiang Yu. Multichannel film dosimetry with nonuniformity correction. *Medical physics*, 38(5):2523–2534, 2011.
- [18] PTW. *Brochure 2016/2017*.
- [19] PTW. *The dose volume calculation algorithm used by OCTAVIUS 4D*.
- [20] PTW. *PTW Detector Arrays Ionization Chambers versus Diodes. A comparison of detectors used in detector arrays*.
- [21] PTW. *User manual farmer chamber ionization chamber type 30010, 30011, 30012, 30013*.
- [22] Min Rao, Wensha Yang, Fan Chen, Ke Sheng, Jinsong Ye, Vivek Mehta, David Shepard, and Daliang Cao. Comparison of elekta vmat with helical tomotherapy and fixed field imrt: plan quality, delivery efficiency and accuracy. *Medical physics*, 37(3):1350–1359, 2010.
- [23] Sotirios Stathakis, Pamela Myers, Carlos Esquivel, Panayiotis Mavroidis, and Nikos Papanikolaou. Characterization of a novel 2d array dosimeter for patient-specific quality assurance with volumetric arc therapy. *Medical physics*, 40(7), 2013.

- [24] Dirk Wolff, Florian Stieler, Grit Welzel, Friedlieb Lorenz, Yasser Abo-Madyan, Sabine Mai, Carsten Herskind, Martin Polednik, Volker Steil, Frederik Wenz, et al. Volumetric modulated arc therapy (vmat) vs. serial tomotherapy, step-and-shoot imrt and 3d-conformal rt for treatment of prostate cancer. *Radiotherapy and Oncology*, 93(2):226–233, 2009.